Queuosine biosynthetic enzyme, QueE moonlights as a cell division regulator

Samuel A. Adeleye[1], Srujana S. Yadavalli[1]*
[1]Waksman Institute of Microbiology and Department of Genetics, Rutgers University, Piscataway NJ 08854

*Corresponding author
sam.yadavalli@rutgers.edu

Keywords: Queuosine, tRNA modification, cell division, bacteria, stress response, moonlighting protein

Abstract

In many organisms, stress responses to adverse environments can trigger secondary functions of certain proteins by altering protein levels, localization, activity, or interaction partners. *Escherichia coli* cells respond to the presence of specific cationic antimicrobial peptides by strongly activating the PhoQ/PhoP two-component signaling system, which regulates genes important for growth under this stress. As part of this pathway, a biosynthetic enzyme called QueE, which catalyzes a step in the formation of queuosine (Q) tRNA modification is upregulated. When cellular QueE levels are high, it co-localizes with the central cell division protein FtsZ at the septal site, blocking division and resulting in filamentous growth. Here we show that QueE affects cell size in a dose-dependent manner. Using alanine scanning mutagenesis of amino acids in the catalytic active site, we pinpoint particular residues in QueE that contribute distinctly to each of its functions – Q biosynthesis or regulation of cell division, establishing QueE as a moonlighting protein. We further show that QueE orthologs from enterobacteria like *Salmonella typhimurium* and *Klebsiella pneumoniae* also cause filamentation in these organisms, but the more distant counterparts from *Pseudomonas aeruginosa* and *Bacillus subtilis* lack this ability. By comparative analysis of *E. coli* QueE with distant orthologs, we elucidate a unique region in this protein that is responsible for QueE's secondary function as a cell division regulator. A dual-function protein like QueE is an exception to the conventional model of "one gene, one enzyme, one function", which has divergent roles across a range of fundamental cellular processes including RNA modification and translation to cell division and stress response.

Introduction

Moonlighting proteins are multifunctional molecules that challenge the one-gene-one-function paradigm (1–3). They are prevalent across all kingdoms of life, from humans to bacteria. In bacteria, they have been shown to link vital metabolic processes to physiological stress responses such as regulation of cell size (4), adhesion (5–7), bacterial virulence, and pathogenicity (5, 8–10). Moonlighting proteins associated with cell division are particularly intriguing because they connect this fundamental process to many additional networks that can profoundly influence cellular physiology. Specific examples include glucosyltransferases – OpgH in *Escherichia coli* and UgtP in *Bacillus subtilis*, which modulate cell division based on nutrient availability (4, 11, 12). In *E. coli*, DnaA, known for its role in initiating DNA replication,

also acts as a transcription factor regulating gene expression (11). In *B. subtilis*, protein DivIVA has been implicated in chromosome segregation and spore formation apart from its role in cell division (13). Studying moonlighting proteins provides a fascinating path to understanding protein functionality, interactions, and complexity within a cell. While our understanding of moonlighting proteins in bacteria has advanced significantly in recent years, several knowledge gaps and challenges remain in this field of research. One of the primary knowledge gaps is the precise molecular mechanisms underlying moonlighting. While some moonlighting functions have been identified and characterized, we often lack a comprehensive understanding of how a single protein can perform multiple functions.

Our previous work found that an enzyme – QueE – involved in the biosynthetic pathway for queuosine (Q) tRNA modification also plays a role in stress response (14). Q is a hypermodified guanosine that is found ubiquitously at the wobble position of the anticodon loop of specific tRNAs – $tRNA^{His}$, $tRNA^{Tyr}$, $tRNA^{Asp}$, and $tRNA^{Asn}$ (15–18). Q-tRNA modification is crucial to maintain translation fidelity and efficiency (19). It has also been implicated in redox, virulence, development, and cancers (18, 20, 21). Despite its universal distribution and importance, only bacteria are capable of *de novo* synthesis of Q from guanosine triphosphate (GTP), and eukaryotes salvage precursors of Q from diet or gut bacteria (15, 18). In the biosynthesis of Q, three enzymes QueD, QueE, and QueC, are required to produce a vital intermediate $PreQ_0$ (22). Specifically, QueE (also called 7-carboxy-7-deazaguanine or CDG synthase) catalyzes the conversion of the substrate CPH_4 (6-carboxy-5,6,7,8-tetrahydropterin) to CDG (7-carboxy-7-deazaguanine) (23). The role of QueE in the biosynthesis of Q has been well characterized, and crystal structures of QueE homologs from *Bacillus subtilis*, *Burkholderia multivorans*, and *Escherichia coli* have been solved, providing insights into the catalytic mechanism (24–27). More recently, a second function for QueE has been described during the stress response of *E. coli* cells exposed to sub-MIC levels of cationic-antimicrobial peptides (AMP) (14). During this response, the PhoQ/PhoP two-component signaling system, which plays an important role in sensing antimicrobial peptides and several other signals (28–30) is strongly activated, leading to an increase in QueE expression. When QueE is upregulated in the cell, it binds at the site of cell division and blocks septation. Consequently, *E. coli* cells grow as long heterogeneous filaments ranging from a few microns to hundreds of microns in length. It has been shown that QueE localizes to the septal Z-ring, a vital structure in bacterial cell division, inhibiting septation post-Z ring formation in an SOS-independent manner (31). This QueE-mediated filamentation phenotype is also observed under other conditions that activate the PhoQ/PhoP system robustly, such as when cells lacking MgrB (a negative feedback inhibitor of PhoQ (32, 33)) are grown under magnesium limitation. Although initially considered a sign of death, filamentation can be a crucial adaptive response to stress (34–37).

In this study, using QueE as a model, we investigate the molecular determinants that allow a protein to perform two distinct functions. We analyze QueE's dual roles in tRNA modification and cell division by utilizing a specialized northern blotting technique and microscopy, respectively, as readouts. By examining single alanine mutants and variants of *E. coli* QueE (*Ec*QueE), we establish that the catalytic activity required for QueE's biosynthetic role is dispensable for its function as a cell division regulator. As a corollary, we identify several individual amino acid residues and a specific region in *Ec*QueE, which are necessary to cause filamentation but not for Q biosynthesis. Analysis of QueE homologs from different bacteria shows that the moonlighting functions of QueE are conserved among other enterobacteria, suggesting this mode of cell division regulation is widespread.

Results

The enzyme QueE has two functions during stress response in *E. coli*.
QueE is required for *de novo* synthesis of queuosine (Q) tRNA modification in prokaryotes (15, 22, 38) as it catalyzes one of the three steps required to form prequeuosine 0 ($preQ_0$), a crucial intermediate in the Q-biosynthetic pathway. Previous work has also shown that QueE mediates the stress response of *E. coli* cells when exposed to sub-lethal concentrations of a cationic antimicrobial peptide, C18G (14). Specifically, as part of this novel secondary function, QueE directly binds to the cell division complex, hindering septation and leading to cell elongation and filamentation (Fig. 1A). To study the molecular determinants in QueE contributing to its dual functions, we utilize two distinct readouts (Fig. 1b). Firstly, to test QueE's function in the formation of Q modification, we adapted published methods based on a specialized gel containing N-acryloyl-3-aminophenylboronic acid (APB) and northern blotting to detect queuosinylated tRNAs (Q-tRNAs) (39, 40). In this technique (APB gel and northern blotting), modified Q-tRNAs containing cis-diol reactive groups migrate slower than unmodified guanosinylated-tRNA (G-tRNAs) (40). Secondly, to examine QueE's ability to cause filamentation, we use phase contrast microscopy and monitor cell morphology. As expected, Δ*queE* cells carrying an empty vector show a band corresponding to unmodified guanosinylated-$tRNA^{Tyr}$ (G-$tRNA^{Tyr}$) but not queuosinylated-$tRNA^{Tyr}$ (Q-$tRNA^{Tyr}$), confirming that QueE is required to produce Q (Fig. 1c). As a positive control, complementation of Δ*queE* cells with WT QueE restores the formation of intact Q-$tRNA^{Tyr}$. Regarding cell morphology, cells lacking QueE do not filament, however, Δ*queE* cells induced to express WT QueE show filamentation (Fig. 1d, (14)). In the following sections, we use the two methods mentioned above to assess the activities of different variants and orthologs of QueE.

QueE regulates cell length in a dose-dependent manner.
Expression of *queE* is upregulated during filamentation of *E. coli* cells in response to sub-lethal concentrations of a cationic antimicrobial peptide, C18G (14). These elongated cells vary from ~2 to hundreds of microns in length, with an average size of ~20 μm. Interestingly, *queE* expression from an IPTG-inducible promoter on a plasmid in wild-type (WT) cells also causes filamentation. To systematically examine the effect of increasing QueE expression on cell length, we performed an IPTG titration using the inducible plasmid encoding *E. coli* QueE (*Ec*QueE) in MG1655 Δ*lacZYA* cells. As the IPTG concentration is increased from 0 to 500 μM, we observe a significant increase in the mean cell length, ranging from approximately 3 to 25 μm, respectively (Fig. 2). The average cell lengths of 18-25 μm obtained for 250-500 μM of IPTG are comparable to those observed for WT cells grown in the presence of sub-MIC level of cationic antimicrobial peptide or Δ*mgrB* cells starved for Mg^{2+}(14). In the absence of IPTG, there is a leaky expression of *queE* encoded by the plasmid, which is similar to the level of gene expression from a genomic copy. As such, the cell length obtained for the strain containing *queE* on plasmid without induction is comparable to that of the cells carrying an empty vector. It is to be noted that the average cell lengths at higher levels of induction are likely underestimated due to the technical limitations in fitting some of the long filaments into the imaging window during microscopy. Overall, our data show a gradual and exponential increase in the extent of filamentation with induction. To confirm if higher induction indeed results in increased levels of QueE protein in cells, we cloned and expressed a His_6-tagged *Ec*QueE on an IPTG-inducible plasmid. This construct behaves similarly to our untagged QueE in causing filamentation upon induction and allows us to monitor His_6-*Ec*QueE levels at different inducer concentrations (Fig. S1a-b). Consistent with our expectation, higher IPTG concentrations correlate with higher amounts of His_6-*Ec*QueE in cells as visualized by western blotting (Fig. S1c-d). As an added control, we show that the His_6-*Ec*QueE maintains the biosynthetic activity

to produce Q-tRNAs (Fig. S1e). Collectively, these results show that QueE levels modulate cell division frequency in a dose-dependent manner.

QueE's function in queuosine-tRNA biosynthesis is independent of its role as a cell division regulator.

Previous genetic analysis has shown that the cellular filamentation phenotype observed during the stress response is QueE-dependent but independent of the other components involved in Q synthesis (14). We wondered if QueE's role in regulating cell division is functionally linked to its activity as a Q biosynthetic enzyme. In other words, does the catalytic active site of QueE contribute to its ability to inhibit septation? To answer this question, we selected amino acid residues in *Ec*QueE vital for Q synthesis based on the crystal structure (27) and performed alanine scanning mutagenesis (Fig. 3a-b). Amino acids Q13, E15, and R27 participate in substrate binding, three Cys residues – C31, C35, and C38 bind iron-sulfur clusters, T40 binds magnesium, and residues G94, S136, and Q189 are involved in cofactor (S-adenosyl methionine) binding [27]. We also included in our analysis three lysine residues identified to be acetylation sites in *Ec*QueE – K60, K66, and K194 (41–43).

We cloned the selected single alanine mutants of QueE on an IPTG-inducible plasmid and expressed each variant in a Δ*queE* background. We then analyzed the effect of each mutant on Q-tRNA production and cell morphology using APB gel-northern blotting (39, 40) and microscopy, respectively (Fig. 3, S2). Notably, mutations at several positions believed to be important for catalysis (Q13, T40, G94, S136, and Q189) and acetylation of QueE (K60 and K194) have a negligible effect on either function (Fig. S2). While an individual mutation may affect the catalytic speed or efficiency of QueE, in this study, we are interested in the overall effect of a mutation in QueE on the formation of the end product (modified Q-tRNA) as a proxy for a functional biosynthetic enzyme. Therefore, these mutations were not considered for further analysis.

Interestingly, one of the mutants, QueE R27A, abolished Q-tRNA formation but retained the ability to cause filamentation like the WT (Fig. 3c-d, S2). The C38A mutation also prevents Q-tRNA formation, however, expression of this mutant does not lead to filamentation, suggesting that the mutation may disrupt overall protein structure and stability. To further characterize the cellular localization of the R27A mutant, we created an N-terminally-tagged YFP-QueE-R27A fusion. The YFP-QueE-WT clone behaves similarly to the untagged protein in modulating septation (14) and is functional in Q-biosynthesis (Fig. S2d). The R27A construct localizes to the Z-ring similarly to the localization of the WT (Fig. 4a, (14)). In addition, the mean length of the filamenting cells observed for the R27A mutant is comparable to that of WT, even though the fluorescence signal for the R27A mutant suggests a somewhat lower level of its expression relative to the WT (Fig. 4c-d). QueE-mediated filamentation also occurs when cells lacking MgrB – a negative feedback inhibitor of PhoQ) – are grown in low magnesium conditions (14). Consistent with our expectation, the QueE-R27A mutant mimics the WT QueE in restoring filamentation in a Δ*mgrB* Δ*queE* strain (Fig. 4b).

In contrast to the R27A mutant, we identified four mutants, E15A, C31A, C35A, and K66A, which do not affect Q-tRNA synthesis but selectively impair the ability to inhibit septation. To cause a block in cell division, QueE needs to be expressed at high levels, so it is possible that these mutants suppressing filamentation are expressed at levels insufficient to hinder division. To determine the expression levels of these individual mutants, we measured fluorescence by incorporating each mutation into the YFP-tagged QueE background. Both mutants, YFP-QueE-C31A and YFP-QueE-C35A, display fluorescence at a level comparable to or higher than YFP-QueE-WT, indicating that the lack of filamentation in strains expressing these mutants is not due

to a lower amount of protein in cells (Fig. S2c). YFP-QueE-E15A and YFP-QueE-K66A show very low fluorescence indicating that these mutations affect protein stability. Yet, it is important to note that the low expression levels seen for the E15A and K66A mutants are sufficient for Q-tRNA synthesis. In conclusion, we have identified and described single amino acid residues in *Ec*QueE that specifically affect either its function in Q-tRNA biosynthesis or cell division. Together, our results establish that the role of QueE as a modulator of septation is independent of its function in the Q-biosynthetic pathway.

Dual functions of QueE are conserved among *E. coli* and related bacteria.
Consistent with the fact that *de novo* biosynthesis of Q is a characteristic of most prokaryotes (38), QueE is widely conserved among bacteria (18, 38, 44). Although the role of *E. coli* QueE (*Ec*QueE) in Q biosynthesis is well established (27), the homolog from *Bacillus subtilis* (*Bs*QueE) was the first to be characterized in terms of its biochemical properties and detailed catalytic mechanism (22, 45, 46). Intriguingly, these two enzymes are less than 40% similar ((14, 27), Fig. S3). Accordingly, QueE homologs across bacterial genera appear to be highly divergent in terms of their gene and protein sequences, resulting in distinct clusters based on sequence similarity analysis (27). QueE protein sequences are increasingly dissimilar as we move farther from enterobacteriaceae within bacterial phylogeny. Therefore, we hypothesized that the sequence divergence among QueE orthologs may impact their functions in Q-tRNA biosynthesis and/or regulation of cell division. To test this hypothesis, we selected and analyzed orthologs of QueE from other gamma proteobacteria – *Klebsiella pneumoniae* (*Kp*QueE), *Salmonella Typhimurium* (StQueE), *Pseudomonas aeruginosa* (*Pa*QueE), and a firmicute, *Bacillus subtilis* (BsQueE). Based on the multiple sequence alignment of selected QueE orthologs and the corresponding phylogenetic tree (Fig. S3), as expected *Bs*QueE is the most distant ortholog, followed by *Pa*QueE.

To test the ability of each QueE ortholog to synthesize Q-tRNAs and inhibit cell division, we cloned each gene into an IPTG inducible multicopy plasmid and induced expression in *E. coli* Δ*queE* cells. All of the QueE orthologs tested here are functional in producing tRNAs modified with Q (Fig. 5a), indicating that this function is well-conserved among these orthologs. However, when we observe the morphology of cells expressing these orthologs, interestingly, only *Kp*QueE and *St*QueE trigger inhibition of septation, but *Bs*QueE and *Pa*QueE do not, when expressed in *E. coli* Δ*queE* cells (Fig. 5b). We considered the possibility that heterologous expression of *Bs*QueE and *Pa*QueE may affect their folding and stability. So, we analyzed the expression of these two QueE orthologs using the YFP-tagged protein fusions along with *Ec*QueE as a control. Upon expression, both YFP-*Bs*QueE and YFP-*Pa*QueE show similar levels of fluorescence as that of YFP-*Ec*QueE (Fig. 5c).

While expression of orthologous proteins in *E. coli* is convenient, it is not testing their function in the native environment where additional factors, which may help cause filamentation, are missing. To test this scenario, we expressed each QueE ortholog on a plasmid in its original host, i.e., *Bs*QueE in *B. subtilis* cells, *Pa*QueE in *P. aeruginosa* cells, and so on. As observed for expression in *E. coli*, *Kp*QueE and *St*QueE cause filamentation in their corresponding host cells, however, *Bs*QueE and *Pa*QueE fail to do so (Fig. S4). Notably, *B. subtilis* and *P.aeruginosa* cells show cell elongation and/or chaining to varying extents irrespective of QueE expression but there is no change in average cell lengths with increased QueE expression (Fig. S4b). Taken together, these results show that the ability of QueE to disrupt cell division is specific to enterobacterial counterparts, closely related to that of *E. coli*.

A distinct region (E45-W67) in *E. coli* QueE is dispensable for its role in queuosine-tRNA biosynthesis but not for the regulation of septation.

Besides sequence variation, the QueE enzyme family also displays a high degree of structural divergence (27), suggesting a molecular basis for the differences observed in the ability of QueE orthologs to regulate cell division. Among the selected QueE proteins, *Bs*QueE and *Pa*QueE do not cause filamentation. *Bs*QueE and *Pa*QueE protein sequences share an identity of only ~19%, 24%, respectively, and <40% similarity with *Ec*QueE (based on EMBOSS Needle pairwise sequence alignments (47), yet they are catalytically active in Q-tRNA synthesis (Fig. 5, S4). To gain insights into the mechanism, we generated a structural alignment to compare the structures of *Ec*QueE (27), *Bs*QueE (46), and an AlphaFold (48, 49) model of *Pa*QueE (Fig. 6a). We see that the catalytic core region corresponding to QueE's CDG synthase activity is preserved between the three QueE proteins despite low sequence similarity Fig. 6, (27). Unsurprisingly, amino acid residues involved in substrate and co-factor binding are well-conserved in the orthologs (Fig. S3a). Based on the structural alignment, we noted a distinguishing feature of *Ec*QueE in the region spanning 22 amino acids E45 through W67 (Fig. 6). According to the *Ec*QueE crystal structure, this region comprises two helical motifs – aT2 and a2', connected to each other and the rest of QueE *via* flexible loops (27). This E45-W67 region from *Ec*QueE appears to be variable among other orthologs, where it is truncated or almost entirely missing in *Bs*QueE and *Pa*QueE (Fig. 6a). We hypothesized that this region with the two helices unique to *Ec*QueE contributes to its second function in inhibiting septation yet dispensable for its Q-biosynthetic function. To test this idea, we cloned *Ec*QueE variants lacking regions comprising either of the helices aT2 (ΔE45-E51), a2' (ΔV52-W67), or both (ΔE45-W67) and expressed them in Δ*queE* cells. Remarkably, *Ec*QueE mutants carrying deletions of either aT2, a2', or the entire region E45-W67 are fully functional in Q-tRNA production (Fig. 6b), indicating that the E45-W67 region is dispensable for Q biosynthesis. However, when we observed the cell morphology, none of the deletion constructs caused filamentation (Fig. 6c), supporting our hypothesis that the E45-W67 region mediates its role in cell division regulation. To control for the possibility that the deletion of this region affects overall protein stability and level in the cell, we quantified protein levels using a YFP-QueE-ΔE45-W67 construct by monitoring cell fluorescence. We see that the level of fluorescence for YFP-QueE-ΔE45-W67 is comparable to that of WT (Fig. 6d).

Given the ability to cause filamentation by *St*QueE and *Kp*QueE, closely related orthologs to *Ec*QueE, we wondered if there is a consensus sequence that can predict whether a given QueE sequence may confer an ability to inhibit cell division. We identify several conserved residues using bioinformatic analysis of QueE protein sequences from 18 representative enterobacteria (Fig. S5). To better represent the amino acid diversity at each position, we generated a WebLogo (50) corresponding to the E45-W67 region in *Ec*QueE, revealing significant features of this sequence (Fig. 7). In particular, amino acids Glu or Asp at position 45, Ile or Val at position 57, Lys60, Thr61, Glu or Asp at position 63 and Trp67 (based on *Ec*QueE numbering) are highly conserved suggesting that their occurrence correlates with QueE's ability to impair septation.

Discussion

Moonlighting proteins highlight the versatility and adaptability of bacterial proteins (1–3, 8, 51). Studying these multifunctional proteins in a model organism such as *E. coli* provides a deeper understanding of protein functionality. Bacterial cell division is a complex process orchestrated primarily by the essential proteins that form the divisome, with FtsZ being one of the most central and well-studied (52–56). However, in addition to these core proteins, there are non-essential, auxiliary proteins that, while not strictly required for cell division, play supportive roles

in regulating the process. A notable example is SulA, an inhibitor of FtsZ polymerization induced in response to DNA damage to temporarily halt cell division (54, 57–59). Accessory proteins, SlmA and Noc, ensure division occurs at appropriate sites and not over the chromosome (60–63). These and several other auxiliary proteins, while "non-essential", can be crucial for survival to fine-tune and ensure optimal cell division under a variety of conditions in natural environments (64–66).

The enzyme QueE, known for its role in Q biosynthesis (67), also regulates septation (14). While QueE-dependent filamentation is not linked to the Q-biosynthetic pathway, it was unclear how QueE performs these two unrelated functions. Here, we show that the regulation of cell size is dependent on the levels of QueE. We find that as QueE expression increases, the average cell length also increases. Using site-directed mutagenesis of catalytically important amino acid residues in *Ec*QueE (27), we identify specific residues that selectively affect filamentation or Q-biosynthesis. In particular, the QueE-R27A mutant is catalytically dead for Q-biosynthesis yet modulates septation. Like the WT, QueE-R27A localizes with FtsZ and the Z-ring, indicating that the septal localization is still maintained in this mutant that is catalytically inactive for Q-biosynthesis. Thus, QueE's role in queuosine biosynthesis and modulation of cell division are not functionally linked, elucidating QueE as a moonlighting protein (Fig. 7).

Based on the structural alignment of QueE orthologs, we observe that the catalytic core domain required for Q biosynthesis is well-preserved (Fig. 6, (27)) and the expression of different QueE enzymes in an *E. coli ⊿queE* strain restores Q-tRNA synthesis (Fig. 5). However, some peripheral structural elements, especially the regions surrounding the iron-sulfur cluster binding pocket, show remarkable variation among members of the QueE family ((27) Fig. 6, S3a). Our results are consistent with the previous analysis that the sequence and structural diversity among QueE proteins do not impact its catalytic function or cofactor binding. Interestingly, Grell et al., ponder over the significance of such large variation in QueE structures. They show that differences in surface elements of QueE as a radical SAM enzyme are at least in part a likely outcome of co-evolution with the cognate flavodoxin that allows for efficient protein-protein interactions (27). Here, we note a stark variation in the region encompassing the two helices α2' and αT2 based on our structural comparison of *Ec*QueE, *Bs*QueE and *Pa*QueE (AlphaFold-generated model). We propose these variable features may explain whether or not a given QueE protein has a moonlighting function. A particular region of interest – comprising E45 through W67 – distinctive to *Ec*QueE, is dispensable for Q biosynthesis but required to cause filamentation (Fig. 6). Specific amino acids in this region are highly conserved among enterobacterial genera (Fig. 7) and potentially mediate the interactions between QueE and proteins at the Z-ring during cell division. We demonstrate that in bacteria from at least three distinct genera, elevated expression of the native QueE ortholog leads to filamentous cell growth (Fig. 5). This indicates that such a mechanism for cell division regulation is widely conserved among Enterobacteriaceae. Two other distant homologs from *P. aeruginosa* and *B. subtilis*, exhibiting lower sequence and structural similarity to *Ec*QueE than enterobacterial orthologs, do not show functional conservation in regulating septation. The target(s) that QueE binds to and the mechanism by which it controls septation are subjects of ongoing inquiry.

Overall, bacteria possess diverse, species-specific regulators that modulate physiological responses based on environmental conditions or the cell's metabolic state. QueE serves as an example to underscore the intricate ways in which bacteria have evolved to use proteins in multiple roles, ensuring efficient coordination between processes like cell division and other essential cellular functions.

Materials and Methods

Strains and plasmids

Details of the strains, plasmids, and oligonucleotides used in this study are provided in the supplemental material (Table S1). *E. coli* K-12 MG1655 strain and its derivatives, plasmid pEB52, and its derivatives were gifts from Dr. Mark Goulian. The following strains, *Pseudomonas aeruginosa* PA01, *Klebsiella pneumoniae* ATCC 13883, *Bacillus subtilis* 168, and *S. Typhimurium* 14208, were gifts from Drs. Bryce Nickels, Huizhou Fan, Jeffrey Boyd, and Deiter Schifferli; plasmid pEG4 was a gift from Dr. Kenn Gerdes.

Media, reagents, and growth conditions

Routine bacterial growth on solid agar was performed using LB Miller medium (IBI scientific) containing 1.5% bacteriological grade agar (VWR Lifesciences) at 37°C. Liquid cultures were grown at 37 °C with aeration in either LB miller medium or minimal A medium (MinA) (K_2HPO_4 (10.5 g l^{-1}), KH_2PO_4 (4.5 g l^{-1}), $(NH_4)_2SO_4$ (10.0 g l^{-1}), Na_3 citrate.$2H_2O$ (0.5 g l^{-1}), supplemented with 0.1% casamino acids, 0.2% glucose and 1 mM concentration of $MgSO_4$ unless otherwise indicated. Throughout this study, MinA supplemented, as indicated above, will be referred to as minimal medium. Antibiotics were used at final concentrations of 100 µg mL^{-1} (LB) or 50 µg mL^{-1} (minimal medium) for carbenicillin and 25 µg mL^{-1} for chloramphenicol. The lac/trc and araBAD promoters were induced using 500 µM b-isopropyl-D-thiogalactoside (IPTG) and 0.3% arabinose, respectively, unless otherwise specified.

For microscopy experiments, overnight cultures of strains harboring specified plasmids were grown in minimal medium (supplemented MinA as described above) and appropriate antibiotics, then back diluted (1:500) into fresh medium unless otherwise indicated. About 4-6 µL of cells were immobilized on glass slides containing agarose pads made from 1% agarose in 1X MinA salts. For the phase contrast microscopy, back-diluted cells were grown for 2 hours (OD_{600} ~0.2) and then induced for 3 hours with either 0.5 mM IPTG or 0.3% arabinose. Cells were grown under the same conditions to detect modified and unmodified tRNA using APB northern blotting. For the fluorescence microscopy and protein localization, SAM96 (*DqueE*) cells expressing either YFP-QueE (pSY76) or YFP-QueE-R27A (pSA58) and FtsZ-mCherry (pEG4) into SAM96 were grown for 4 hours, followed by addition of arabinose and growth for another 1 hour to reach OD_{600} ~0.4-0.5. To monitor single-cell fluorescence in cells expressing QueE and its variants, SAM96 cells containing plasmids (pSA57, pSA58, pSY76, pSA73, pSA75, pSA76, pSA119, pSA121, pSA126) were grown for 5 hours to reach OD_{600} 0.4-0.5. In fluorescence quantification experiments, the cultures were rapidly cooled in an ice slurry, and streptomycin was added at 250 µg mL^{-1} to halt translation. For IPTG titration experiments, overnight cultures of TIM183/pRL03 or TIM183/pSY85 and TIM183/pTra99a were back diluted (1:500) into fresh medium. These cells were grown for 2 hours and then induced with IPTG at concentrations 0, 10, 25, 50, 75, 100, 250, and 500 µM for 3 hours, followed by imaging.

Cloning of QueE and its variants

Plasmids encoding single alanine mutants of *E. coli* QueE, His_6-QueE, and YFP-QueE were made using inverse PCR or single primer methods using pRL03 (untagged QueE), His_6-QueE (pSY85) or YFP-QueE (pSY76) EcQueE as templates. QueE orthologs from *S. Typhimurium* 14028 and *Pseudomonas aeruginosa* PA01 were cloned using restriction sites, EcoRI and BamHI, while *Bacillus subtilis* QueE was cloned using the SacI and BamHI restriction sites in a pEB52 vector resulting in the plasmids pSA21, pSA22, and pSY45 respectively. Since *K. pneumoniae* ATCC 13883 has an intrinsic resistance to ampicillin/carbenicillin, the QueE gene from *K. pneumoniae* was cloned into a pBAD33 vector using the Xba1 and Kpn1 restriction sites

to create plasmid pSA59. We also added a ribosome binding site (RBS) to pBAD33, upstream of the start site of the cloned gene using the inverse PCR cloning method. Plasmids pSA60, pSA61, and pSA62 encoding variants of *E. coli* QueE, QueE-ΔE45-E51, QueE-ΔV52-W67, and QueE-ΔE45-W67 were made using inverse PCR. YFP-tagged *Bs*QueE and *Pa*QueE were made using the NEB Hi-Fi Assembly protocol by substituting *Ec*QueE in the pSY76 background. All constructs were confirmed by Sanger sequencing, and plasmids were transformed into chemically competent *E. coli* Top10 or XL1-Blue strains for maintenance in 20% glycerol at -80°C. Plasmids were transformed into MG1655 and its derivatives (TIM183, SAM31, or SAM96) as applicable.

Microscopy and image analysis

Phase contrast and fluorescence microscopy of MG1655 Δ*queE* (SAM96 or SAM31) cells harboring plasmids of QueE, single alanine mutants, QueE orthologs, and their variants were performed as previously described (14). 4-6 µL of the cells were immobilized on 1% agarose pads, and their morphology was observed using a Nikon TiE fluorescent microscope with a TI2-S-HU attachable mechanical stage. The images were captured using a Teledyne Photometrics Prime 95B sCMOS camera with 1x1 binning. The Nikon Ti-E's perfect focus system (PFS) ensured continuous focus during imaging. YFP and mCherry fluorescent images were taken with a 100 ms exposure time at 20% intensity, while phase-contrast images were captured with a 40 ms exposure time and 20% intensity. All image acquisition during experiments was managed using Metamorph software version 7.10.3.279. The background fluorescence was determined using the MG1655 Δ*queE* (SAM96) strain grown under the same conditions. The average cell fluorescence was quantified using ImageJ and the MicrobeJ plugin. Data from independent replicates was plotted using R.

APB gel electrophoresis and northern blotting

$tRNA^{Tyr}$ modified with queuosine (Q) in total cell RNA was detected using previously published protocols (39, 40) with the following modifications. Total RNA was extracted from cell pellets using the Trizol RNA extraction method (68). 150 ng of total RNA was deacylated in 100 mM Tris-HCl (pH 9.0) at 37°C for 30 minutes. The deacylated RNA was run on a 0.4 mm thick ~~0.4 mM~~ 7% Urea denaturing polyacrylamide gel, supplemented with 0.5% 3-acrylamidophenylboronic acid (APB). The RNA was transferred using a semi-dry system to a Nytran SuPerCharge nylon blotting membrane (VWR). After transfer, the membrane was crosslinked twice using a UV crosslinker (Fisher Scientific) at optimal conditions (254 nm wavelength and 1200 mJ energy) and hybridized in 50 mL hybridization buffer (750 mM NaCl and 75 mM sodium citrate, 20 mM Na_2HPO_4, 7% SDS, 0.04% BSA fraction V (high purity), 0.04% Ficoll 400, and 0.04% polyvinylpyrrolidone) at pH 7.0, supplemented with 200 µL sheared salmon sperm DNA (10 mg/mL). Following hybridization for 1 hour, $5'$-^{32}P labeled oligonucleotides with complementarity to $tRNA^{Tyr}$ were added and incubated for 16-18 hours at 50 °C. The blot was washed thoroughly with a low-stringent wash solution (450 mM NaCl and 45 mM sodium citrate, 25 mM Na_2HPO_4 (pH 7.2), 5% SDS, 0.2% BSA fraction V (high purity), 0.2% Ficoll 400, 0.2% polyvinylpyrrolidone, and DEPC ddH_2O) at 50°C for 15 minutes each, and once with stringent wash solution (150 mM NaCl and 15 mM sodium citrate, 1% SDS, DEPC ddH_2O) at 50°C for 5 minutes. The blot was exposed to a phosphor imager screen and imaged using the phosphorimager (GE Amersham™ Typhoon) at a sensitivity of 4000.

Cell lysate preparation and western blotting

Cell pellets harvested from 25 mL cultures of TIM183/pSY85 grown in the absence or presence of varying concentrations of inducer (IPTG) were resuspended in 400 µL 20% sucrose/30 mM Tris pH 8.0. and 1 mL 3mM EDTA pH 7.2 was added. The cells were sonicated for ~30 sec (10-sec pulse, 10-sec gap, 3x) using a sonicator (Fisher Scientific, VCX-130 Vibra-Cell Ultrasonic).

The resulting lysed cells were centrifuged at 600rpm for 5 minutes, and the supernatant was collected for further use. Each sample is normalized by the cellular biomass and loaded onto two 12% Bis tris gels using MES as a running buffer at 160V for 1 hour. One gel is stained using the Coomassie gel protocol, destained, and imaged using a Biorad Gel Doc XR+ System, while the other was processed for western blotting. Separated proteins were transferred to a PVDF membrane (Amersham™ Hybond™ P 0.2 µm) in a transfer buffer supplemented with 20% methanol. The His_6-QueE is detected with an anti-His primary antibody and IRDye-conjugated secondary antibody (LI-COR). The protein bands were visualized with the Odyssey CLx imaging system (LI-COR).

Sequence and structural analysis
The protein sequences of QueE orthologs were obtained from Ecocyc (69). Multiple sequence alignments were performed using Clustal Omega, and the phylogenetic tree diagrams were generated using Jalview (70). The consensus sequence was generated using Weblogo (50, 71). The structural model of *Pa*QueE was computed using AlphaFold (48, 49), and the structural alignment of *Bs*QueE, *Ec*QueE, and *Pa*QueE was generated using Pymol (72).

Data availability

The data underlying this article are available in the article and in the supplementary data.

Funding

Srujana S. Yadavalli is supported by NIGMS R35 GM147566 and institutional start-up funds. Samuel A. Adeleye was supported by a Waksman Institute Busch Predoctoral Fellowship.

Conflict of interest statement. Srujana S. Yadavalli consults for and collaborates with Designs for Vision Inc.

Acknowledgments

The authors would like to thank Drs. Mark Goulian, Bryce Nickels, Huizhou Fan, Dieter Schifferli, Jeffrey Boyd and Kenn Gerdes for generously sharing strains and plasmids. We thank the past and present members of the Yadavalli and Shah Labs for helpful discussions. We also thank Drs. Premal Shah, and Manuela Roggiani for critical reading of the manuscript.

Figures

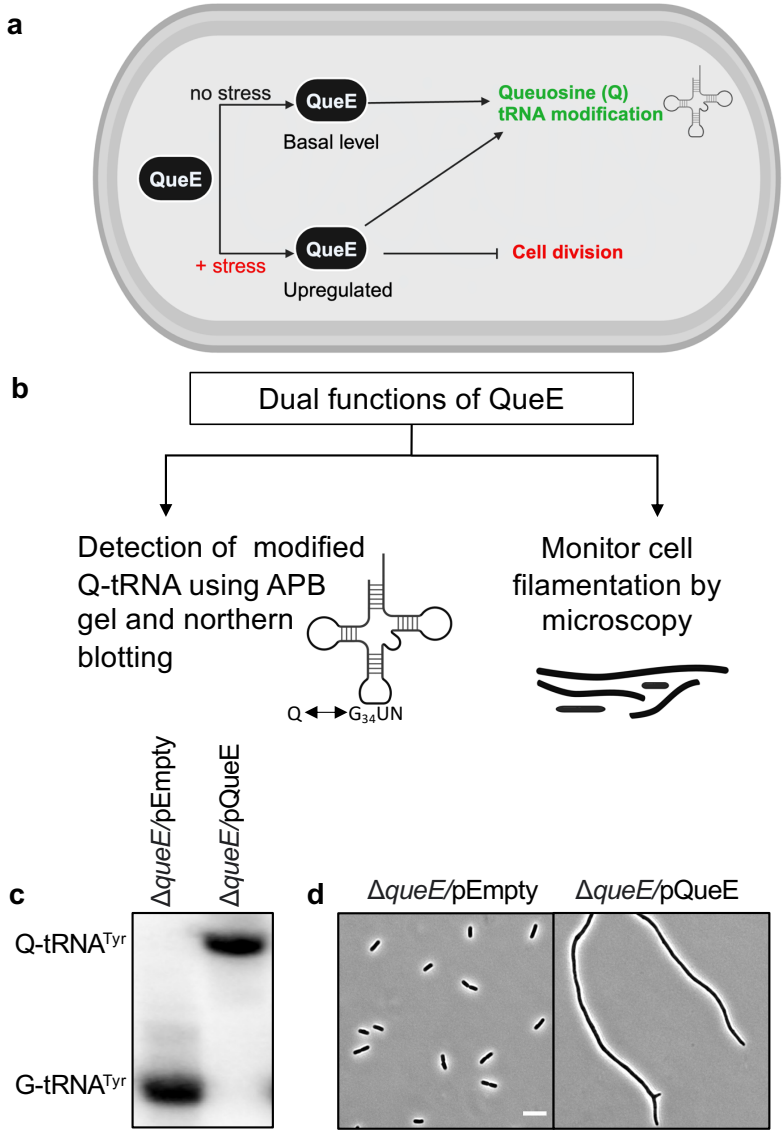

Figure 1. Dual functions of E. coli QueE (EcQueE) during stress response. (a) Schematic representation of the dual roles of QueE. QueE is an enzyme required for the biosynthesis of queuosine (Q) tRNA modification. *E. coli* cells under antimicrobial peptide stress upregulate QueE, which then modulates cell division in addition to Q biosynthesis. (b) Methods used to study the two functions of QueE – APB (N-acryloyl-3-aminophenylboronic acid) gel and northern blotting to detect Q-tRNAs and microscopy to observe filamentation. (c) APB gel-northern blot detecting $tRNA^{Tyr}$ in total RNA samples of Δ*queE* (SAM31) cells encoding either an empty vector (pEB52) or wild-type (WT) QueE (pRL03). G-$tRNA^{Tyr}$ = unmodified $tRNA^{Tyr}$, Q-$tRNA^{Tyr}$ = Q-modified $tRNA^{Tyr}$. (d) Representative phase-contrast micrographs of Δ*queE* (SAM31) cells expressing either an empty vector (pEB52) or WT QueE (pRL03) scale bar = 5 μm.

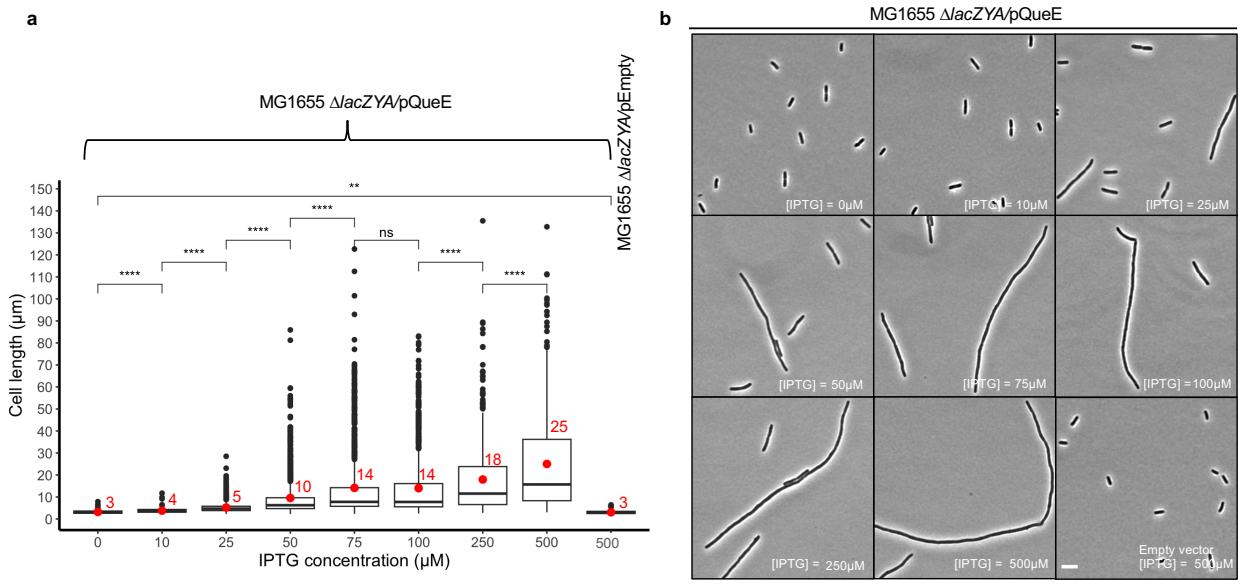

Figure 2. QueE regulates septation in a dose-dependent manner. (a) Measurement of cell lengths of *E. coli* MG1655 Δ*lacZYA* (TIM183) cells expressing QueE. Strains containing a plasmid encoding *E. coli* QueE (pRL03) or empty vector (pEB52) were grown in minimal medium containing 1 mM Mg^{2+} for 2 hours (OD_{600} = 0.2-0.3) and induced with IPTG for 3 hours at the indicated concentration. Mean cell length values are indicated in red, and the horizontal black bars represent the median. Data are obtained from four independent experiments using at least 350 cells for each inducer concentration. Statistical analysis was done using t-test displaying significance at *P ≤ 0.05, **P ≤ 0.01, ***P ≤ 0.001, ****P ≤ 0.0001, and "ns" = P >0.05 (b) Representative phase-contrast micrographs of Δ*lacZYA* cells expressing QueE (pRL03) at the indicated inducer concentration, scale bar = 5 μm.

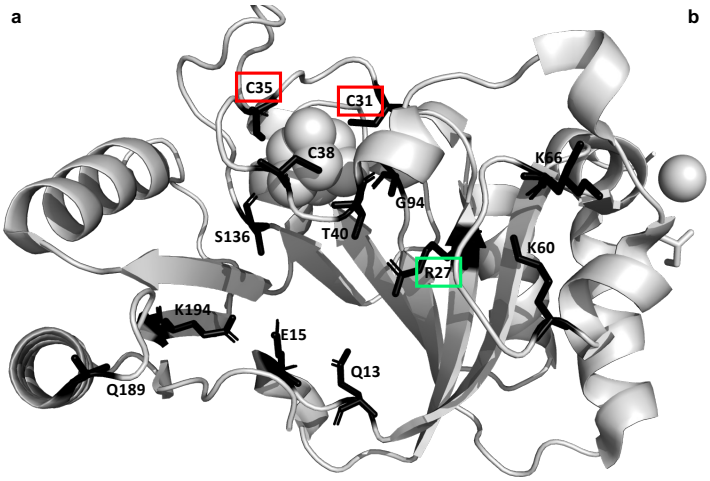

b

Amino acids	Role	Cell Morphology	Q-tRNA synthesis
Q13	Substrate binding	F	Q
E15	Substrate binding	NF	Q
R27	Substrate binding	F	NQ
C31	[4Fe-4S] cluster	NF	Q
C35	[4Fe-4S] cluster	NF	Q
C38	[4Fe-4S] cluster	NF	NQ
T40	Magnesium binding	F	Q
K60	Acetylation site	F	Q
K66	Acetylation site	NF	Q
G94	SAM cofactor binding	F	Q
S136	SAM cofactor binding	F	Q
Q189	SAM cofactor binding	F	Q
K194	Acetylation site	F	Q

Key: F= Filamenting, NF= Non-filamenting, Q= Q produced, NQ= No Q produced

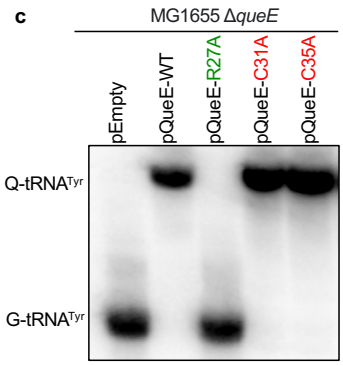

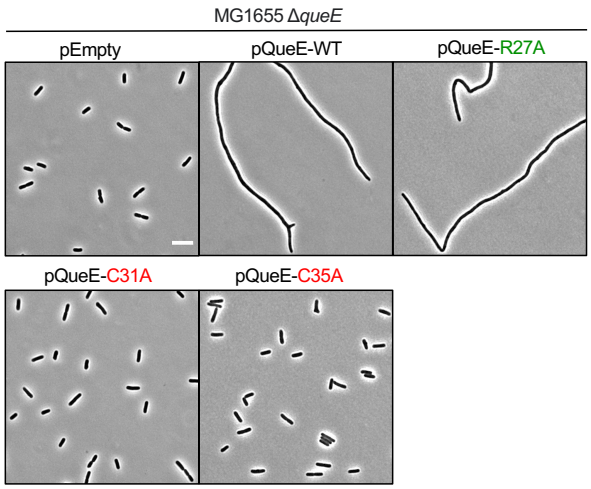

Figure 3. Mutation of conserved amino acid residues in *Ec*QueE affect either Q biosynthesis or cell division. (a) Structure of *E. coli* QueE (EcQueE, PDB ID 6NHL) showing amino acid residues, catalytically important for Q biosynthesis. (b) Summary of alanine scanning mutagenesis of key amino acid residues in *Ec*QueE and the effect of each mutant on cellular morphology and Q biosynthesis. (c) APB gel-northern blot detecting $tRNA^{Tyr}$ in total RNA samples of Δ*queE* (SAM31) cells encoding either WT QueE (pRL03), QueE-R27A (pSY98), QueE-C31A (pSA1), QueE-C35A (pSA2) or an empty vector (pEB52). G-$tRNA^{Tyr}$ = unmodified $tRNA^{Tyr}$, Q-$tRNA^{Tyr}$ = Q-modified $tRNA^{Tyr}$. (d) Representative phase-contrast micrographs of Δ*queE* (SAM31) cells expressing WT QueE and selected mutants, scale bar = 5 μm.

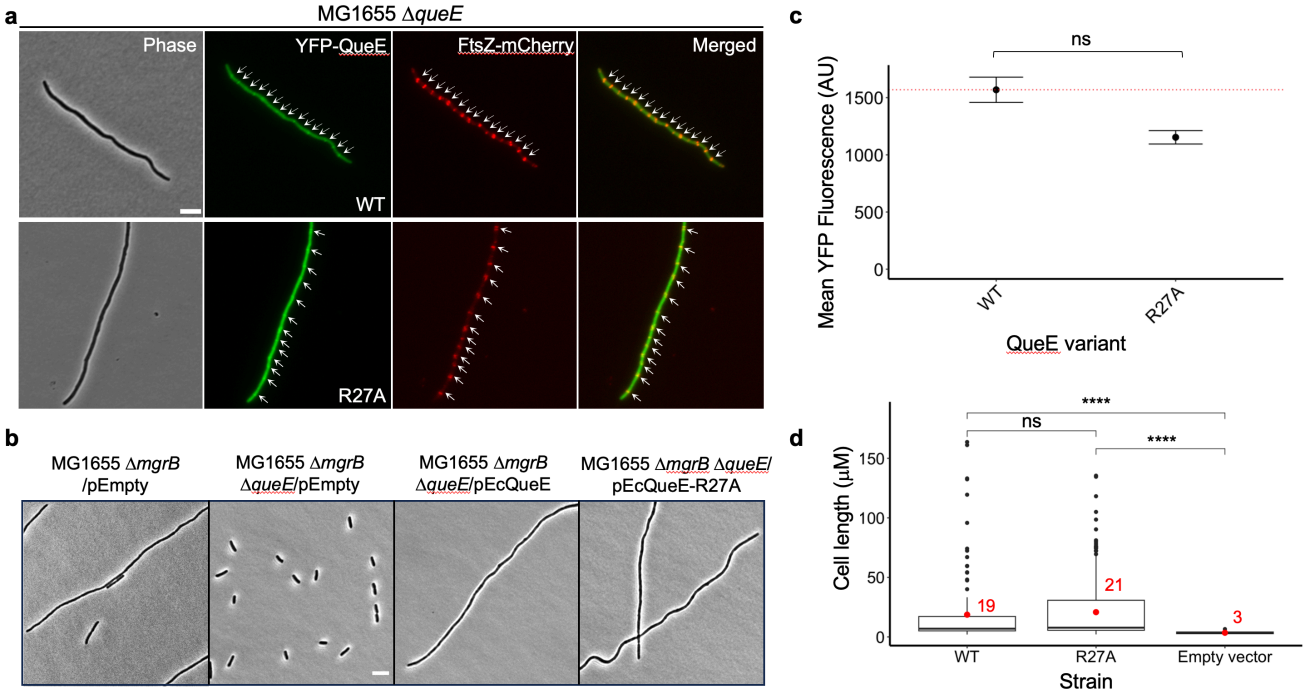

Figure 4. *Ec*QueE-R27A mutant, deficient in Q biosynthesis, retains the ability to control cell division. (a) Representative phase-contrast and fluorescence micrographs of Δ*queE* (SAM96) cells co-expressing FtsZ-mCherry (pEG4) and either YFP-EcQueE (pSY76) or YFP-*Ec*QueE-R27A (pSA58). Green and red arrowheads represent the localization of YFP-QueE and FtsZ- mCherry, respectively. (b) Representative phase-contrast micrographs of Δ*mgrB* and Δ*mgrB*Δ*queE* cells containing either an empty plasmid (pEB52), or plasmids expressing *Ec*QueE (pRL03) and *Ec*QueE-R27A (pSY98), scale bar = 5 μm. (c) Quantification of YFP-QueE levels in Δ*queE* (SAM96) cells transformed with plasmids encoding YFP-tagged WT *Ec*QueE (pSY76), *Ec*QueE-R27A (pSA58), or an empty vector (pEB52). Data represent the mean and range from two independent experiments and fluorescence was quantified from ≥ 50 cells per individual sample. The red dotted line represents the expression level for WT YFP-QueE (d) Measurement of cell lengths of Δ*queE* (SAM96) cells encoding WT *Ec*QueE (pRL03), *Ec*QueE-R27A (pSY98), or an empty vector (pEB52). Mean cell length values are indicated in red and the horizontal black bars represent the median. Data are obtained from three independent experiments using at least 125 cells for each strain. Statistical analysis was done using t-test displaying significance at *P ≤ 0.05, **P ≤ 0.01, ***P ≤ 0.001, ****P ≤ 0.0001, and "ns" = P >0.05.

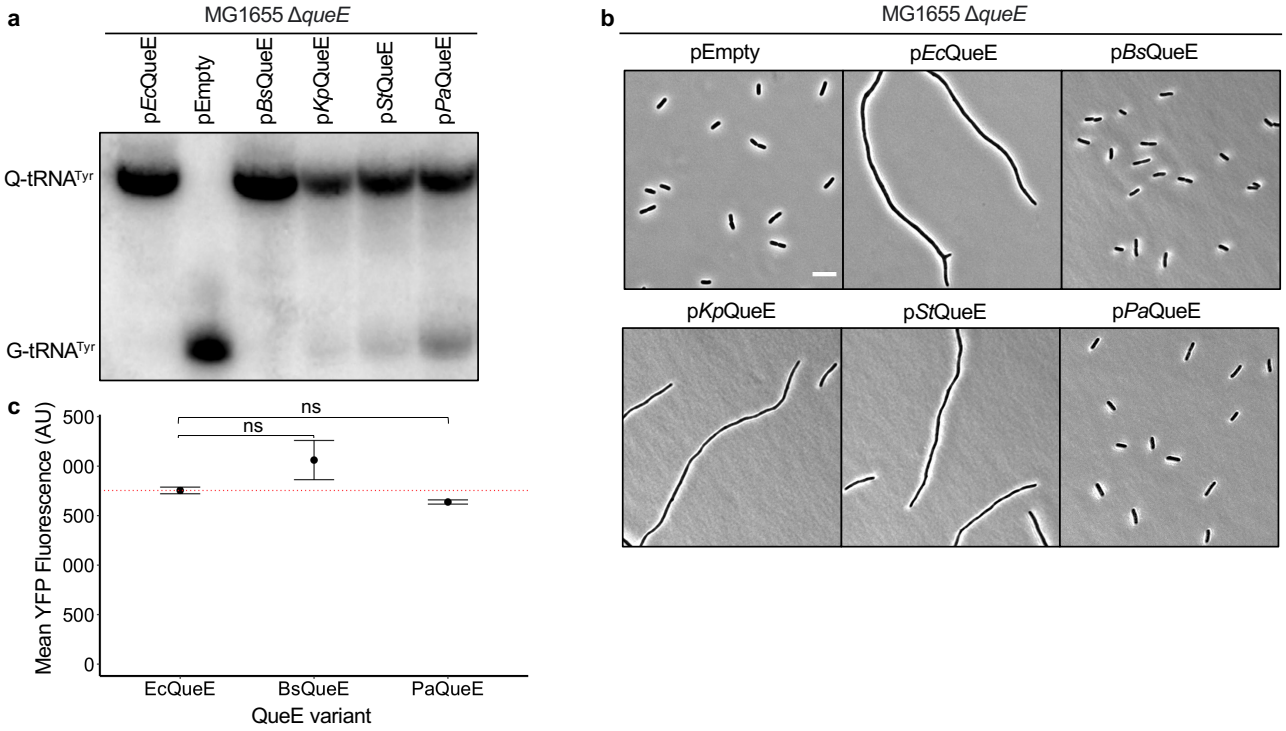

Figure 5. Dual functions of QueE are conserved among orthologs from *E. coli* and closely related genera. (a) APB gel-northern blot detecting $tRNA^{Tyr}$ in total RNA samples of Δ*queE* (SAM31) cells encoding QueE orthologs from *E. coli* (*Ec*QueE, pRL03), *Bacillus subtilis* (*Bs*QueE, pSY45), *Klebsiella pneumoniae* (*Kp*QueE, pSA5), *Salmonella Typhimurium* St1408 (*St*QueE, pSA21), *Pseudomonas aeruginosa* PA01(*Pa*QueE, pSA127) and an empty vector (pEB52). G-$tRNA^{Tyr}$ = unmodified $tRNA^{Tyr}$, Q-$tRNA^{Tyr}$ = Q-modified $tRNA^{Tyr}$. (b) Representative phase-contrast micrographs of Δ*queE* (SAM31) cells transformed with plasmids encoding either *Ec*QueE, *Bs*QueE, *Kp*QueE, *St*QueE, p*Pa*QueE, or an empty vector, scale bar = 5μm. (c) Quantification of YFP-QueE levels in Δ*queE* (SAM96) cells transformed with plasmids encoding YFP-tagged *Ec*QueE (pSY76), *Bs*QueE (pSA121), *Pa*QueE (pSA126), or an empty vector (pEB52). Data represent the mean and range from two independent experiments, and fluorescence was quantified from ≥ 150 cells per individual sample. The red dotted line represents the expression level for WT YFP-QueE, Statistical analysis was done using t-test displaying significance at *P ≤ 0.05, **P ≤ 0.01, ***P ≤ 0.001, ****P ≤ 0.0001, and “ns” = P >0.05.

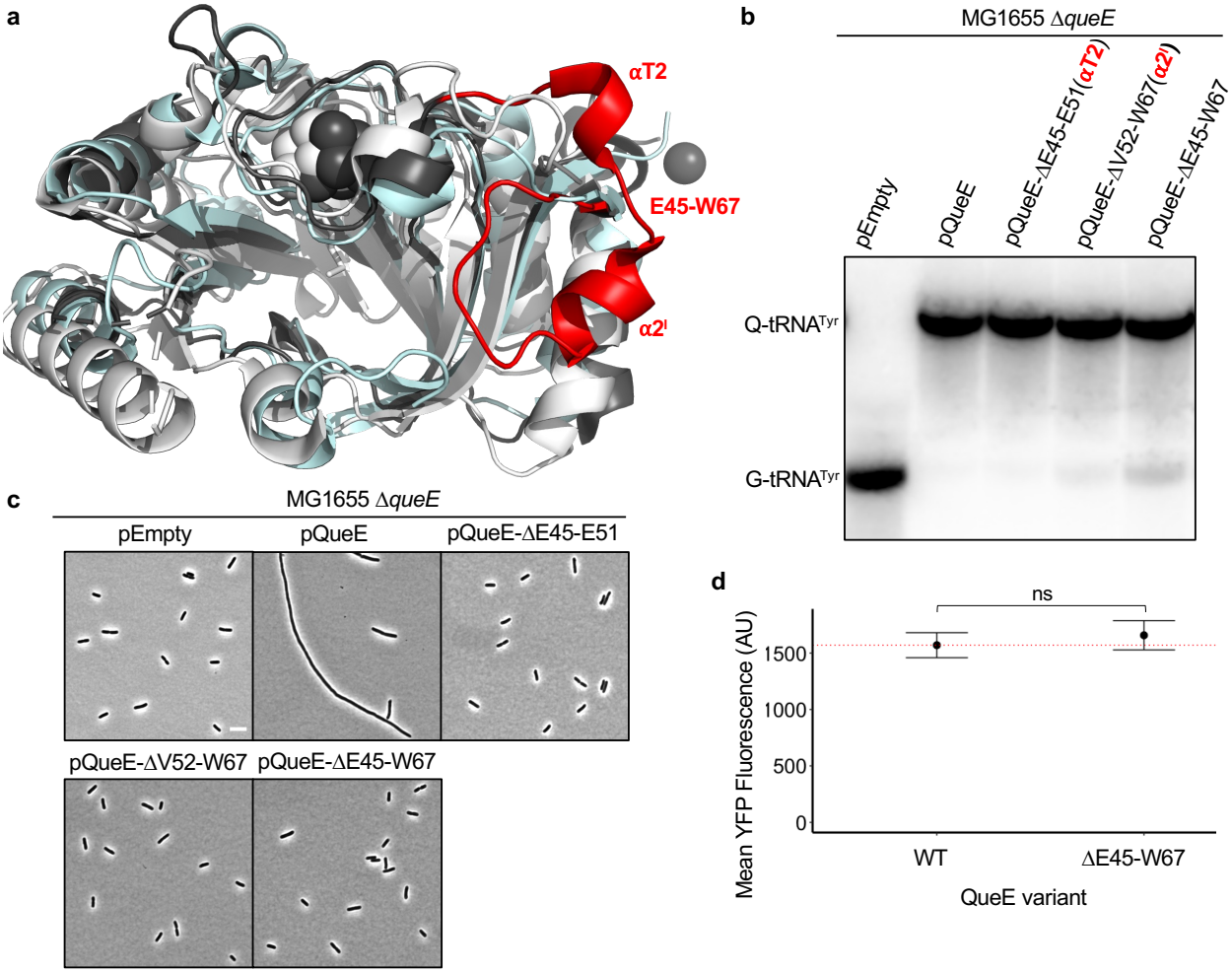

Figure 6. Region E45-W67 in *E. coli* QueE is dispensable for the biosynthesis of Q-tRNA modification. (a) Structural alignment of *E. coli* QueE (*Ec*QueE, PDB 6NHL, dark gray), *Bacillus subtilis* QueE (*Bs*QueE, PDB 5TH5, light gray), and an Alphafold-generated model of *P. aeruginosa* QueE (*Pa*QueE, cyan). The variable region E45-W67 in *Ec*QueE is highlighted in red. (b) APB gel-northern blot showing Q-tRNA profiles of ΔqueE cells (SAM31) containing IPTG inducible plasmids encoding *E. coli* QueE (pRL03), control vector (pEB52), and selected mutants of *Ec*QueE - pQueE-ΔE45-E51 (pSA60), pQueE-ΔV52-W67 (pSA61), and pQueE-ΔE45-W67 (pSA62). G-tRNA^{Tyr} = unmodified tRNA^{Tyr}, Q-tRNA^{Tyr} = Q-modified tRNA^{Tyr} (c) Phase contrast micrographs of Δ*queE* (SAM31) cells transformed with an empty vector and plasmids encoding Wildtype (WT) *Ec*QueE and the selected *Ec*QueE peptide deletion mutants (as in (a) above), Scale bar = 5 µm. (d) Quantification of QueE levels in Δ*queE* (SAM96) cells transformed with an empty vector and IPTG inducible plasmids encoding YFP tagged Wildtype (WT) QueE (pSY76) and QueE-ΔE45-W67 (pSA76). Dots and the error bars represent the mean and range from two independent experiments with quantified fluorescence from ≥ 50 cells. The red dotted line represents the expression levels for WT (Filamenting, synthesize Q). Statistical analysis was done using t-test displaying significance at *P ≤ 0.05, **P ≤ 0.01, ***P ≤ 0.001, ****P ≤ 0.0001, and “ns” = P >0.05.

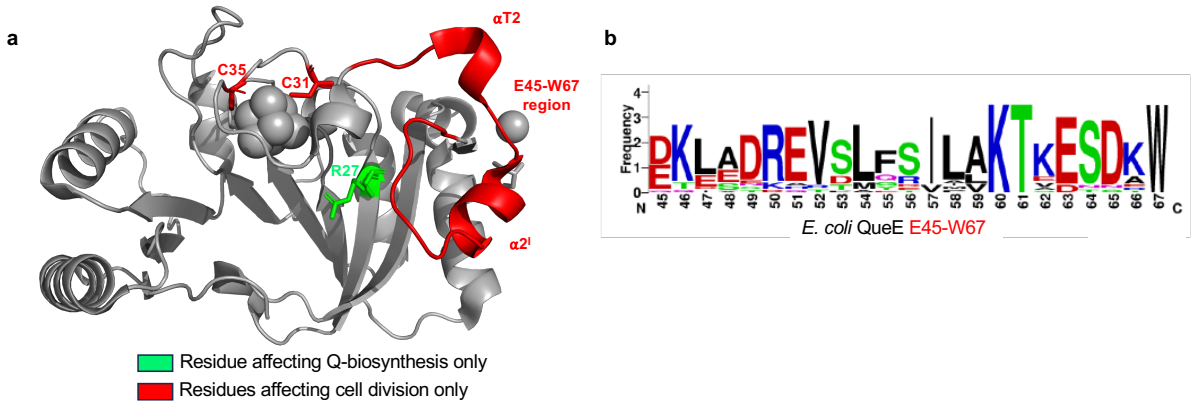

Figure 7. QueE's dual roles in Q-biosynthesis and septation inhibition. (a) Structure of *E. coli* QueE (PDB 6NHL) showing residue affecting Q-biosynthesis only (green, R27) and septation inhibition only (red, C31, C35, E45-W67). (b) A consensus sequence of the E45-W67 region from 18 representative enterobacteria (see Fig. S6 for details) was generated using WebLogo (50).

Supporting Information

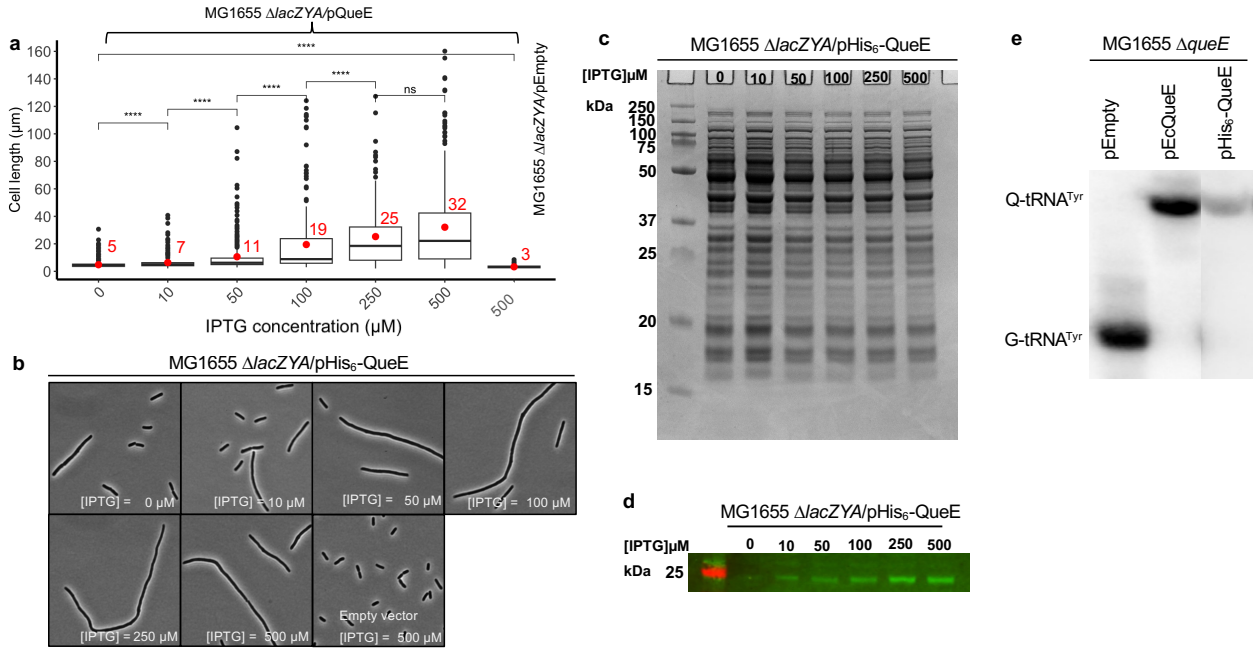

Figure S1. His$_6$-tagged QueE regulates septation in a dose-dependent manner. (a) Measurement of cell lengths of *E. coli* MG1655 Δ*lacZYA* (TIM183) cells expressing QueE. Strains containing a plasmid encoding *E. coli* His$_6$-*Ec*QueE (pSY85) or empty vector (pEB52) were grown in minimal medium containing 1 mM Mg^{2+} for 2 hours (OD_{600} = 0.2-0.3) and induced with IPTG for 3 hours at the indicated concentration. Mean cell length values are indicated in red, and the horizontal black bars represent the median. Data are obtained from four independent experiments using at least 180 cells for each inducer concentration. Statistical analysis was done using t-test displaying significance at *P ≤ 0.05, **P ≤ 0.01, ***P ≤ 0.001, ****P ≤ 0.0001, and "ns" = P >0.05 (b) Representative phase-contrast micrographs of Δ*lacZYA* cells expressing QueE at the indicated inducer concentration, scale bar = 5 µm. (c-d) A Coomassie gel showing protein levels in total cell lysates at different IPTG concentrations and a western blot showing the corresponding His$_6$-QueE levels. e) APB gel-northern blot detecting $tRNA^{Tyr}$ in total RNA samples of Δ*queE* (SAM31) cells encoding either WT QueE (pRL03), his$_6$-QueE (pSY85) or an empty vector (pEB52). G-$tRNA^{Tyr}$ = unmodified $tRNA^{Tyr}$, Q-$tRNA^{Tyr}$ = Q-modified $tRNA^{Tyr}$.

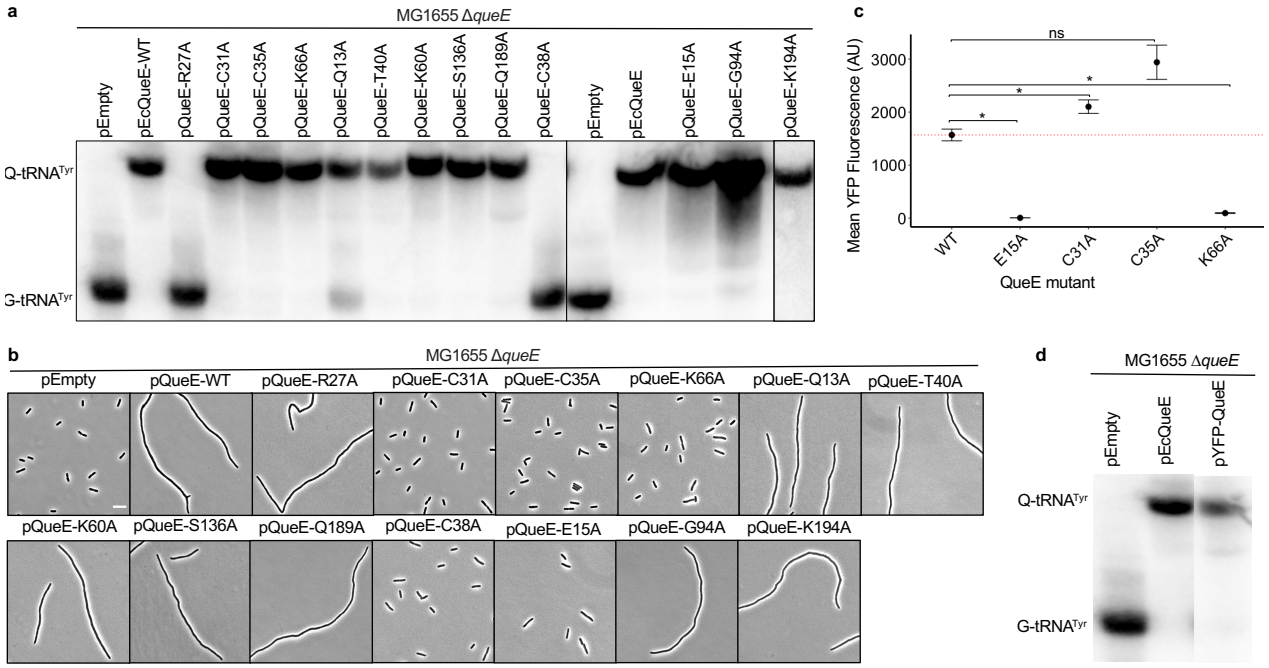

Figure S2. Alanine scanning mutagenesis of amino acid residues in *Ec*QueE important for Q biosynthesis. (a) APB northern blot detecting $tRNA^{Tyr}$ in total RNA samples of Δ*queE* (SAM31) cells encoding either WT QueE (pRL03), QueE variants, QueE-R27A (pSY98), QueE-C31A (pSA1), QueE-C35A (pSA2.6), QueE-K66A (pSA10), QueE-Q13A (pSY97), QueE-T40A (pSY99), QueE-K60A (pSA9), QueE-S136A (pSA8), QueE-Q189A (pSY100), QueE-C38A (pSA3) or an empty vector (pEB52). G-$tRNA^{Tyr}$ = unmodified $tRNA^{Tyr}$, Q-$tRNA^{Tyr}$ = Q-modified $tRNA^{Tyr}$. (b) Representative phase-contrast micrographs of Δ*queE* (SAM31) cells expressing WT QueE and single alanine mutants as indicated above in (a), scale bar = 5 µm. (c) Quantification of levels of YFP-tagged QueE and its variants in Δ*queE* (SAM96) cells transformed with plasmids encoding WT YFP-QueE (pSY76), YFP-QueE-E15A (pSA73), YFP-QueE-C31A (pSA75), YFP-QueE-C35A (pSA119), or YFP-QueE-K66A (pSA57). Data represent the mean and range from two independent experiments, and fluorescence was quantified from ≥ 50 cells per individual sample. The red dotted line represents the expression level for WT YFP-QueE, Statistical analysis was done using t-test displaying significance at *P ≤ 0.05, **P ≤ 0.01, ***P ≤ 0.001, ****P ≤ 0.0001, and “ns” = P >0.05. (d) APB gel- northern blot detecting $tRNA^{Tyr}$ in total RNA samples of Δ*queE* (SAM31) cells encoding either WT QueE (pRL03), YFP-QueE (pSY76) or an empty vector (pEB52). G-$tRNA^{Tyr}$ = unmodified $tRNA^{Tyr}$, Q-$tRNA^{Tyr}$ = Q-modified $tRNA^{Tyr}$.

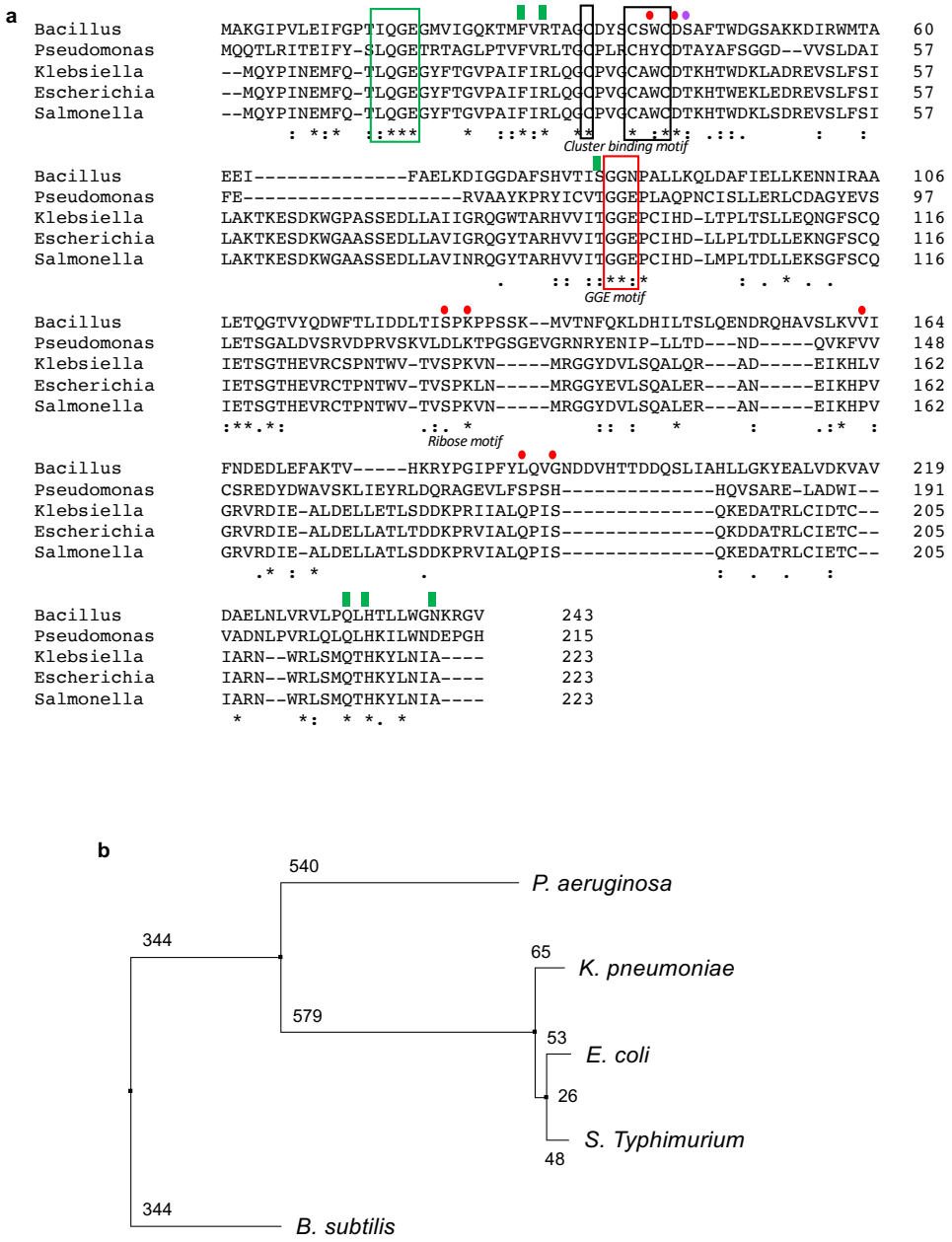

Figure S3. Sequence analysis and phylogeny of selected QueE orthologs. (a) Multiple sequence alignment of QueE orthologs from *Bacillus subtilis* str 168, *Pseudomonas aeruginosa* PA01, *Klebsiella pneumoniae*, *Escherichia coli K-12 MG1655*, and *Salmonella Typhimurium* St1408. The cluster binding motif residues are boxed in black, and residues involved in binding S-adenosyl methionine are highlighted using red circles (single residues) and red boxes (sequential residues). Residues involved in substrate binding (CPH_4/6-CP ligation) are denoted by green rectangles (single residues) and green boxes (sequential residues). A single amino acid residue involved in binding the catalytic magnesium ion is indicated by a purple circle. (b) Phylogenetic tree of the QueE orthologs estimated by the neighbor-joining method (BLOSUM62) using Jalview (Waterhouse et al 2009).

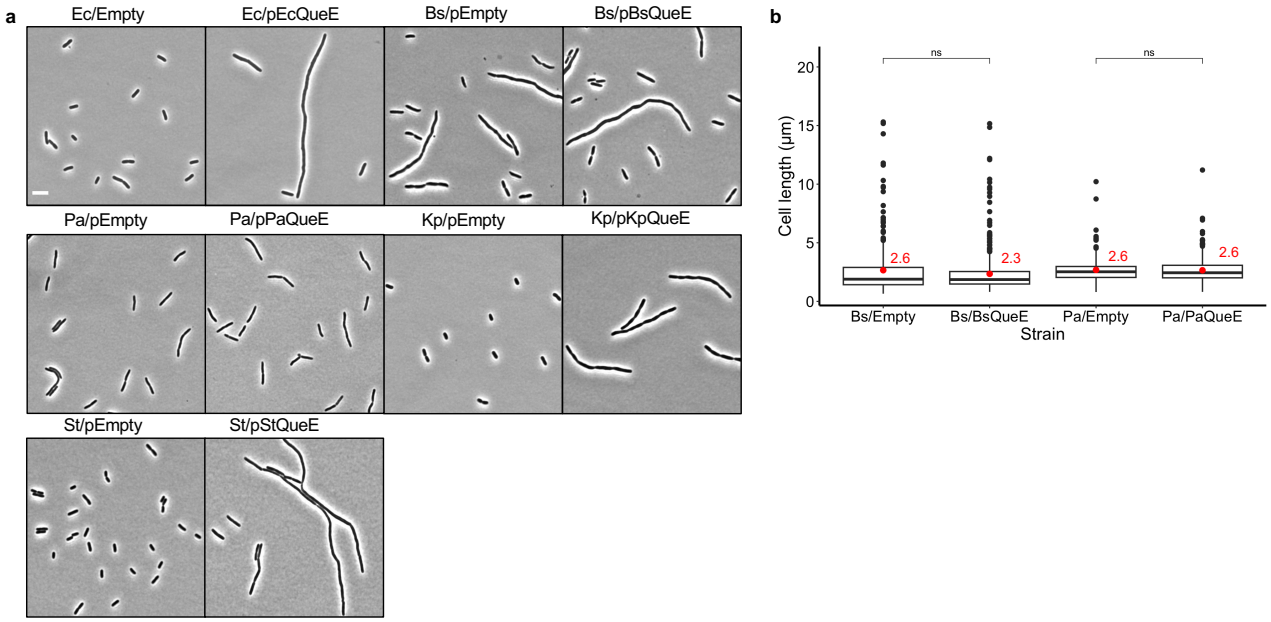

Figure S4. Analysis of dual functions of *Ec*QueE orthologs in their hosts. (a) Representative phase-contrast micrographs of *E. coli, Bacillus subtilis*, *Klebsiella pneumoniae*, *Salmonella Typhimurium* St1408, and *Pseudomonas aeruginosa* PA01 expressing their native QueE ortholog *Ec*QueE (pRL03), *Bs*QueE (pSY45), *Kp*QueE (pSA59), *St*QueE (pSA21), *Pa*QueE (pSA127), respectively, or an empty vector (pEB52 or pBAD33), scale bar = 5µm. (b) Measurement of cell lengths of *Bacillus subtilis* and *Pseudomonas aeruginosa* PA01 cells expressing *Bs*QueE, and *Pa*QueE, respectively, or an empty vector. Mean cell length values are indicated in red, and the horizontal black bars represent the median. Data are obtained from two independent experiments using at least 277 cells for each strain, Statistical analysis was done using t-test displaying significance at *P ≤ 0.05, **P ≤ 0.01, ***P ≤ 0.001, ****P ≤ 0.0001, and "ns" = P >0.05.

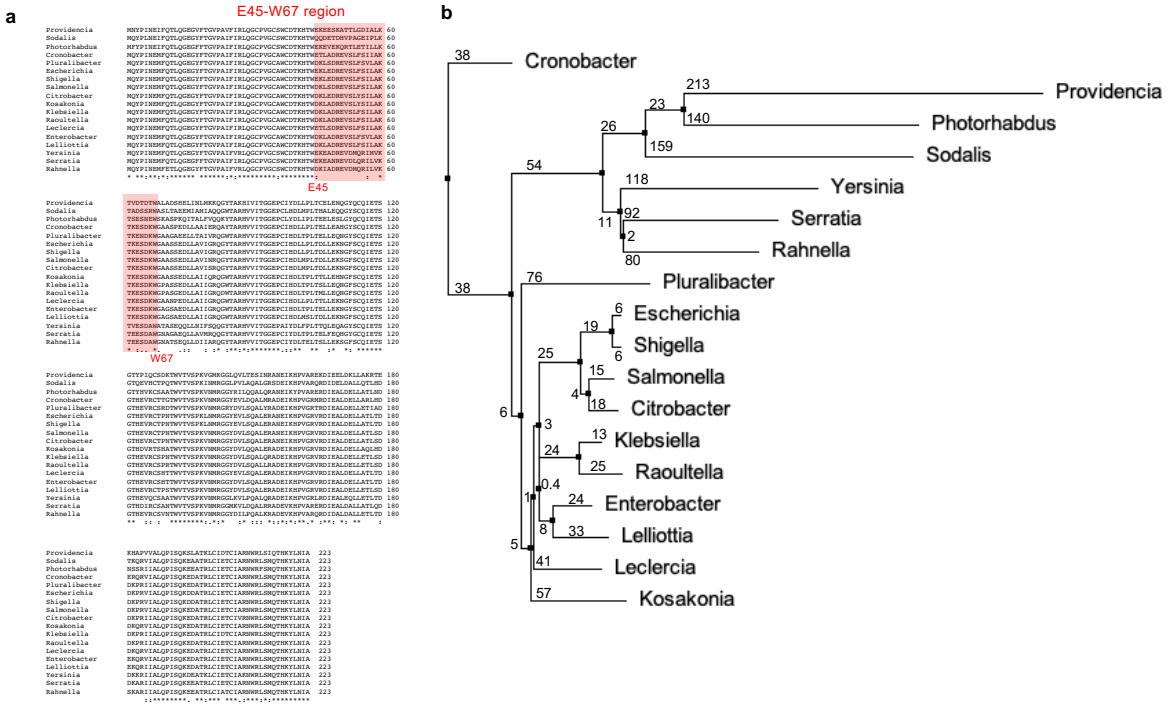

Figure S5. Sequence analysis and phylogeny of selected QueE orthologs from gammaproteobacteria (a) Multiple sequence alignment of 18 QueE orthologs from representative enterobacteria generated using ClustalW. The E45-W67 region is highlighted in red. (b). Phylogenetic tree of the selected QueE sequences estimated by the neighbor-joining method (BLOSUM62) using Jalview (70)

Tables

A. List of strains used in the study

Strain	Relevant genotype	Reference/source
MG1655	λ⁻ rph-1	*E. coli* Genetic Stock Center, CGSC no. 7740
SAM96	MG1655 ΔqueE	(14)
SAM31	MG1655 ΔqueE λatt (PmgrB-yfp) HKatt (PtetA-cfp)	Goulian lab
TIM183	MG1655 ΔlacZYA	
Top10	*F– mcrA Δ(mrr-hsdRMS-mcrBC) φ80lacZΔM15 ΔlacX74 recA1 araD139 Δ(ara-leu)7697 galU galK λ– rpsL (StrR) endA1 nupG*	Invitrogen
XL1-Blue	*recA1 endA1 gyrA96 thi-1 hsdR17 supE44 relA1 lac [F´ proAB lacIqZΔM15 Tn10 (Tetr)]*	(73)
B. subtilis	ind- tyr+	Boyd lab
P. aeruginosa PA01	lacIq+ delta(lacZ)M15+ tetA+ tetR+	Nickels lab
Klebsiella pneumoniae	Klebsiella pneumoniae subsp. pneumoniae (Schroeter) Trevisan 13883	Fan lab
S. Typhimurium 14208	Salmonella enterica subsp. enterica (ex-Kauffmann and Edwards) Le Minor and Popoff serovar Typhimurium, ATCC 14028	Schifferli lab

B. List of plasmids used in the study

Name	Description	Reference/source
pRL03	pEB52-EcQueE, carbR	(14)
pSY85	pEB52-His$_6$-QueE, carbR	This work
pEG4	pBAD33 ftsZ-mCherry, camR	(74)
pSY45	pEB52-BsQueE, carbR	This work
pSA59	pBAD33-KpQueE, camR	This work
pSA21	pEB52-StQueE, carbR	This work
pSA22	pEB52-PaQueE, carbR	This work

pSA1	pEB52-EcQueE, C31A, carbR	This work
pSA2	pEB52-EcQueE, C35A, carbR	This work
pSA3	pEB52-EcQueE, C38A, carbR	This work
pSA5	pEB52-EcQueE, E15A, carbR	This work
pSA8	pEB52-EcQueE, S136A, carbR	This work
pSA9	pEB52-EcQueE, K60A, carbR	This work
pSA10	pEB52-EcQueE, K66A, carbR	This work
pSA11	pEB52-EcQueE, K194A, carbR	This work
pSA55	pEB52-EcQueE, W67A, carbR	This work
pSA60	pRL03- ΔE45-E51, carbR	This work
pSA61	pRL03- ΔV52-W67, carbR	This work
pSA62	pRL03- ΔE45-W67, carbR	This work
pSA119	pEB52-yfp-QueE, C35-A, carbR	This work
pSA73	pEB52- yfp -EcQueE, E15A, carbR	This work
pSA75	pEB52- yfp -EcQueE, C31A, carbR	This work
pSA57	pEB52- yfp -EcQueE, K66A, carbR	This work
pSA58	pEB52- yfp -EcQueE, R27A, carbR	This work
pSA121	pEB52- yfp -pBsQueE, carbR	This work
pSA126	pEB52- yfp -pPaQueE, carbR	This work
pSA76	pEB52- yfp -EcQueE, ΔE45-W67	This work
pSY76	pEB52-yfp-QueE, carbR	(14)
pSY98	pEB52-EcQueE, R27A, carbR	This work
pTrc99a	Ptrc-MCS lacIq, carbR	(75)
pBAD33	ori(p15A), ParaBAD-MCS araC, camR	ATCC 87402
pEB52	pTrc99a with the NcoI site removed, carbR	Goulian lab
pSY100	pEB52-EcQueE, Q189A, carbR	This work
pSY99	pEB52-EcQueE, T40A, carbR	This work

pSY97	pEB52-EcQueE, Q13A, carbR	This work

carbR = carries a carbenicillin/ampicillin-resistance marker; camR = carries a chloramphenicol-resistance marker

C. List of oligonucleotides used in the study

Name of Primer	5' - 3'	Reference/source
SA1	TACAGTCTGCTCCCTTTGGCCGCTCGGGAACC CCAC	Probe for tyrU Gene
SA3F	GCCCCGGTTGGCTGTGCCTG	Inv PCR Primer for C31A
SA3R	TCCCTGTAAACGAATAAAAATGGCGG	Inv PCR Primer for C31A
SA4F	GCCGCCTGGTGCGACACCAAACAC	Inv PCR Primer for C35A
SA4R	GCCAACCGGGCATCCCTGTAAACG	Inv PCR Primer for C35A
SA7F	ACCTTGCAGGGTCTGGAACATCTCG	Inv PCR Primer for E15A
SA7R	GCCGGTTACTTTACCGGCGTTCCCG	Inv PCR Primer for E15A
SA9F	GCCGAGCCTTGCATTCATGATTTGCTGCC	Inv PCR Primer for G94A
SA9R	ACCCGTAATCACCACATGCCGC	Inv PCR Primer for G94A
SA11F	GTTGGCTGTGCCTGGGCCGACACCAAACACAC	Single Primer SDM for C38A in *E. coli* QueE
SA13F	GCCTGGGGGGCTGCGAGCAGTG	Inv PCR Primer for K66A
SA13R	ATCACTCTCTTTGGTCTTCGCCAG	Inv PCR Primer for K66A
SA12F	GCCACCAAAGAGAGTGATAAGTGGG	Inv PCR Primer for K60A
SA12R	CGCCAGAATGCTGAAAAGGGA	Inv PCR Primer for K60A
SA10F	GCCCCAAAGCTGAACATGCGCGGC	Inv PCR Primer for S136
SA10R	TACGGTAACCCAGGTATTCGGTGTGC	Inv PCR Primer for S136
SA5F	GCCGACACCAAACACACCTGGG	Inv PCR Primer for C38A
SA5R	CAGGCACAGCCAACCGGGC	Inv PCR Primer for C38A
queE-Q189A-L1	CAGTGCAATGACTCGCGGTTTATCATC	Inv PCR Primer for Q189A

queE-Q189A-U1	gcgCCGATTAGCCAAAAGGATGATGCCA	Inv PCR Primer for Q189A
queE-T40A-L1	GTCGCACCAGGCACAGCCAAC	Inv PCR Primer for T40A
queE-T40A-U1	gcgAAACACACCTGGGAAAAGCTTGAG	Inv PCR Primer for T40A
queE-R27A-L1	AATAAAAATGGCGGGAACGCCG	Inv PCR Primer for R27A
queE-R27A-U1	gcgTTACAGGGATGCCCGGTTGG	Inv PCR Primer for R27A
queE-Q13A-L1	CAGGGTCTGGAACATCTCGTTAATCG	Inv PCR Primer for Q13A
queE-Q13A-U1	gcgGGTGAGGGTTACTTTACCGGC	Inv PCR Primer for Q13A
SA79F	GCGTTACAGGGATGCCCGGTTGG	R27A F-primer
SA79R	AATAAAAATGGCGGGAACGCCG	R27A R-primer
SA80F	aaattaagcATGCAGTACCCGATTAACGAGATG	Adds RBS to pSA56
SA80R	ctcctctttaatGgtaccgagctcgaattcg	Adds RBS to pSA56
SA26R	CATCCGCCAAAACAGCCAAG	Seq R-Primer for pEB52 inserts
Bs_queE-SacI-U1	GACTACGAGCTCAAAAGGGTGGTTTGAATGGC TAAAG	BsQueE in pEB52
Bs_queE-BamHI-L1	AGTAGTGGATCCCTATTATACTCCGCGTTTGTTG CC	BsQueE in pEB52
SA28F	CAGAGAATTCatgGTTTCAGCTCGGCTGATCTTC	StQueE in pEB52
SA28R	TAGAGGATCCtcaATGGCCCGGTTCGTCG	StQueE in pEB52
SA29F	CAGAGAATTCATGCAGTACCCGATTAACGAAAT GTTCC	PaQueE
SA29R	TAGAGGATCCTCAGGCGATATTTAAATACTTATG CGTTTGC	PaQueE
SA78F	ATTAGGTACCATGCAGTACCCGATTAACGAGAT GTTC	KpQueE in pBAD33
SA78R	ATTATCTAGATCAGGCAATATTCAGATACTTGTG CGTC	KpQueE in pBAD33
SA81F	ggcagcggcGTCTCCCTTTTCAGCATTCTGGCG	Inverse PCR Primer to remove E45-E51 to pRL03
SA81R	gctgccgccCCAGGTGTGTTTGGTGTCG	Inverse PCR Primer to remove E45-E51 to pRL03
SA82F	ggcagcggcGGGGCTGCGAGCAGTGAAG	Inverse PCR Primer to remove V52-W67 to pRL03
SA82R	gctgccgccTTCCCGATCCTCAAGCTTTTCCC	Inverse PCR Primer to remove V52-W67 to pRL03
SA69F	Ccataagattagcggatcctacctgac	pBAD33 Forward sequencing primer

SA69R	tcagaccgcttctgcgttc	pBAD33 Reverse sequencing primer
SA125R_pSY76_R	tctagtTTTGTATAGTTCATCCATGCCATGTG	Hifi assembly vector primer
SA125F_pSY76_Bs	CAACAAACGCGGAGTAtaaTTAAACATTTATAAGCGTTATAAATGGGTGGAACC	Hifi assembly vector primer for BsQueE
SA125F_pSY76_Pa	GAACCGGGCCATtgaTTAAACATTTATAAGCGTTATAAATGGGTGGAACC	Hifi assembly vector primer for PaQueE
SA126F_Bs_F	CATGGATGAACTATACAAAactagaatgGCTAAAGGAATTCCTGTATTAGAAATTTTCGG	Hifi assembly insert primer for BsQueE
SA126R_Bs_R	ttaTACTCCGCGTTTGTTGCCC	Hifi assembly insert primer for BsQueE
SA127F_Pa_R	TTAAtcaATGGCCCGGTTCGTC	Hifi assembly insert primer for PaQueE
SA127R_Pa_Corr_F	CATGGATGAACTATACAAAactagaatgCAACAGACCCTGCGC	Hifi assembly insert primer for PaQueE

References

1. Singh,N. and Bhalla,N. (2020) Moonlighting proteins. *Annu. Rev. Genet.*, **54**, 265–285.

2. Jeffery,C.J. (2014) An introduction to protein moonlighting. *Biochem. Soc. Trans.*, **42**, 1679–1683.

3. Jeffery,C.J. (2015) Why study moonlighting proteins? *Front. Genet.*, **6**, 211.

4. Hill,N.S., Buske,P.J., Shi,Y. and Levin,P.A. (2013) A moonlighting enzyme links Escherichia coli cell size with central metabolism. *PLoS Genet.*, **9**, e1003663.

5. Henderson,B. and Martin,A. (2011) Bacterial virulence in the moonlight: multitasking bacterial moonlighting proteins are virulence determinants in infectious disease. *Infect. Immun.*, **79**, 3476–3491.

6. Kainulainen,V. and Korhonen,T.K. (2014) Dancing to Another Tune—Adhesive Moonlighting Proteins in Bacteria. *Biology* , **3**, 178–204.

7. Jeffery,C. (2018) Intracellular proteins moonlighting as bacterial adhesion factors. *AIMS Microbiol*, **4**, 362–376.

8. Wang,G., Xia,Y., Cui,J., Gu,Z., Song,Y., Chen,Y.Q., Chen,H., Zhang,H. and Chen,W. (2014) The Roles of Moonlighting Proteins in Bacteria. *Curr. Issues Mol. Biol.*, **16**, 15–22.

9. Henderson,B. (2014) An overview of protein moonlighting in bacterial infection. *Biochem. Soc. Trans.*, **42**, 1720–1727.

10. Henderson,B. and Martin,A. (2013) Bacterial moonlighting proteins and bacterial virulence. *Curr. Top. Microbiol. Immunol.*, **358**, 155–213.

11. Levin,P.A. and Angert,E.R. (2015) Small but mighty: Cell size and bacteria. *Cold Spring Harb. Perspect. Biol.*, **7**, a019216.

12. Chien,A.-C., Zareh,S.K.G., Wang,Y.M. and Levin,P.A. (2012) Changes in the oligomerization potential of the division inhibitor UgtP co-ordinate Bacillus subtilis cell size with nutrient availability. *Mol. Microbiol.*, **86**, 594–610.

13. Errington,J. (2003) Regulation of endospore formation in Bacillus subtilis. *Nat. Rev. Microbiol.*, **1**, 117–126.

14. Yadavalli,S.S., Carey,J.N., Leibman,R.S., Chen,A.I., Stern,A.M., Roggiani,M., Lippa,A.M. and Goulian,M. (2016) Antimicrobial peptides trigger a division block in Escherichia coli through stimulation of a signalling system. *Nat. Commun.*, **7**, 12340.

15. Reader,J.S., Metzgar,D., Schimmel,P. and de Crécy-Lagard,V. (2004) Identification of four genes necessary for biosynthesis of the modified nucleoside queuosine. *J. Biol. Chem.*, **279**, 6280–6285.

16. Kersten,H. and Kersten,W. (1990) Chapter 2 Biosynthesis and Function of Queuine and Queuosine tRNAs. In Gehrke,C.W., Kuo,K.C.T. (eds), *Journal of Chromatography Library*. Elsevier, Vol. 45, pp. B69–B108.

17. Nishimura,S. (1983) Structure, biosynthesis, and function of queuosine in transfer RNA. *Prog. Nucleic Acid Res. Mol. Biol.*, **28**, 49–73.

18. Vinayak,M. and Pathak,C. (2009) Queuosine modification of tRNA: its divergent role in cellular machinery. *Biosci. Rep.*, **30**, 135–148.

19. Müller,M., Legrand,C., Tuorto,F., Kelly,V.P., Atlasi,Y., Lyko,F. and Ehrenhofer-Murray,A.E. (2019) Queuine links translational control in eukaryotes to a micronutrient from bacteria. *Nucleic Acids Res.*, **47**, 3711–3727.

20. Hayes,P., Fergus,C., Ghanim,M., Cirzi,C., Burtnyak,L., McGrenaghan,C.J., Tuorto,F., Nolan,D.P. and Kelly,V.P. (2020) Queuine Micronutrient Deficiency Promotes Warburg Metabolism and Reversal of the Mitochondrial ATP Synthase in Hela Cells. *Nutrients*, **12**.

21. Ren,D., Mo,Y., Yang,M., Wang,D., Wang,Y., Yan,Q., Guo,C., Xiong,W., Wang,F. and Zeng,Z. (2023) Emerging roles of tRNA in cancer. *Cancer Lett.*, **563**, 216170.

22. McCarty,R.M., Somogyi,Á., Lin,G., Jacobsen,N.E. and Bandarian,V. (2009) The Deazapurine Biosynthetic Pathway Revealed: In Vitro Enzymatic Synthesis of PreQ0 from Guanosine 5′-Triphosphate in Four Steps. *Biochemistry*, **48**, 3847–3852.

23. McCarty,R.M., Somogyi,A. and Bandarian,V. (2009) Escherichia coli QueD is a 6-carboxy-5,6,7,8-tetrahydropterin synthase. *Biochemistry*, **48**, 2301–2303.

24. Lewis,J.K., Bruender,N.A. and Bandarian,V. (2018) QueE: A Radical SAM Enzyme Involved in the Biosynthesis of 7-Deazapurine Containing Natural Products. *Methods Enzymol.*, **606**, 95–118.

25. Zhu,W. and Liu,Y. (2015) Ring contraction catalyzed by the metal-dependent radical SAM enzyme: 7-carboxy-7-deazaguanine synthase from B. multivorans. Theoretical insights into the reaction mechanism and the influence of metal ions. *ACS Catal.*, **5**, 3953–3965.

26. Bruender,N.A., Grell,T.A.J., Dowling,D.P., McCarty,R.M., Drennan,C.L. and Bandarian,V. (2017) 7-Carboxy-7-deazaguanine Synthase: A Radical.

27. Grell,T.A.J., Bell,B.N., Nguyen,C., Dowling,D.P., Bruender,N.A., Bandarian,V. and Drennan,C.L. (2019) Crystal structure of AdoMet radical enzyme 7-carboxy-7-deazaguanine synthase from Escherichia coli suggests how modifications near [4Fe-4S] cluster engender flavodoxin specificity. *Protein Sci.*, **28**, 202–215.

28. Groisman,E.A. (2016) Feedback Control of Two-Component Regulatory Systems. *Annu. Rev. Microbiol.*, **70**, 103–124.

29. Rao,S.D. and Igoshin,O.A. (2021) Overlaid positive and negative feedback loops shape dynamical properties of PhoPQ two-component system. *PLoS Comput. Biol.*, **17**, e1008130.

30. Groisman,E.A. (2001) The pleiotropic two-component regulatory system PhoP-PhoQ. *J. Bacteriol.*, **183**, 1835–1842.

31. Margolin,W. (2005) FtsZ and the division of prokaryotic cells and organelles. *Nat. Rev. Mol. Cell Biol.*, **6**, 862–871.

32. Lippa,A.M. and Goulian,M. (2009) Feedback inhibition in the PhoQ/PhoP signaling system by a membrane peptide. *PLoS Genet.*, **5**, e1000788.

33. Yadavalli,S.S., Goh,T., Carey,J.N., Malengo,G., Vellappan,S., Nickels,B.E., Sourjik,V., Goulian,M. and Yuan,J. (2020) Functional determinants of a small protein controlling a broadly conserved bacterial sensor kinase. *J. Bacteriol.*, **202**.

34. Horvath,D.J.,Jr, Li,B., Casper,T., Partida-Sanchez,S., Hunstad,D.A., Hultgren,S.J. and Justice,S.S. (2011) Morphological plasticity promotes resistance to phagocyte killing of uropathogenic Escherichia coli. *Microbes Infect.*, **13**, 426–437.

35. Justice,S.S., Hunstad,D.A., Cegelski,L. and Hultgren,S.J. (2008) Morphological plasticity as a bacterial survival strategy. *Nat. Rev. Microbiol.*, **6**, 162–168.

36. Jones,T.H., Vail,K.M. and McMullen,L.M. (2013) Filament formation by foodborne bacteria under sublethal stress. *Int. J. Food Microbiol.*, **165**, 97–110.

37. Abell-King,C., Costas,A., Duggin,I.G. and Söderström,B. (2022) Bacterial filamentation during urinary tract infections. *PLoS Pathog.*, **18**, e1010950.

38. Fergus,C., Barnes,D., Alqasem,M.A. and Kelly,V.P. (2015) The queuine micronutrient: charting a course from microbe to man. *Nutrients*, **7**, 2897–2929.

39. Dineshkumar,T.K., Thanedar,S., Subbulakshmi,C. and Varshney,U. (2002) An unexpected absence of queuosine modification in the tRNAs of an Escherichia coli B strain. *Microbiology*, **148**, 3779–3787.

40. Matuszek,Z. and Pan,T. (2019) Quantification of Queuosine Modification Levels in tRNA from Human Cells Using APB Gel and Northern Blot. *Bio Protoc*, **9**, e3191.

41. Christensen,D.G., Meyer,J.G., Baumgartner,J.T., D'Souza,A.K., Nelson,W.C., Payne,S.H., Kuhn,M.L., Schilling,B. and Wolfe,A.J. (2018) Identification of Novel Protein Lysine Acetyltransferases in Escherichia coli. *MBio*, **9**.

42. Schilling,B., Christensen,D., Davis,R., Sahu,A.K., Hu,L.I., Walker-Peddakotla,A., Sorensen,D.J., Zemaitaitis,B., Gibson,B.W. and Wolfe,A.J. (2015) Protein acetylation dynamics in response to carbon overflow in Escherichia coli. *Mol. Microbiol.*, **98**, 847–863.

43. Kuhn,M.L., Zemaitaitis,B., Hu,L.I., Sahu,A., Sorensen,D., Minasov,G., Lima,B.P., Scholle,M., Mrksich,M., Anderson,W.F., *et al.* (2014) Structural, kinetic and proteomic characterization of acetyl phosphate-dependent bacterial protein acetylation. *PLoS One*, **9**, e94816.

44. Tuorto,F., Legrand,C., Cirzi,C., Federico,G., Liebers,R., Müller,M., Ehrenhofer-Murray,A.E., Dittmar,G., Gröne,H.-J. and Lyko,F. (2018) Queuosine-modified tRNAs confer nutritional control of protein translation. *EMBO J.*, **37**, e99777.

45. McCarty,R.M., Krebs,C. and Bandarian,V. (2013) Spectroscopic, steady-state kinetic, and mechanistic characterization of the radical SAM enzyme QueE, which catalyzes a complex cyclization reaction in the biosynthesis of 7-deazapurines. *Biochemistry*, **52**, 188–198.

46. Bruender,N.A., Grell,T.A.J., Dowling,D.P., McCarty,R.M., Drennan,C.L. and Bandarian,V. (2017) 7-Carboxy-7-deazaguanine Synthase: A Radical S-Adenosyl-l-methionine Enzyme with Polar Tendencies. *J. Am. Chem. Soc.*, **139**, 1912–1920.

47. Madeira,F., Pearce,M., Tivey,A.R.N., Basutkar,P., Lee,J., Edbali,O., Madhusoodanan,N., Kolesnikov,A. and Lopez,R. (2022) Search and sequence analysis tools services from EMBL-EBI in 2022. *Nucleic Acids Res.*, **50**, W276–W279.

48. Jumper,J., Evans,R., Pritzel,A., Green,T., Figurnov,M., Ronneberger,O., Tunyasuvunakool,K., Bates,R., Žídek,A., Potapenko,A., *et al.* (2021) Highly accurate protein structure prediction with AlphaFold. *Nature*, **596**, 583–589.

49. Varadi,M., Anyango,S., Deshpande,M., Nair,S., Natassia,C., Yordanova,G., Yuan,D., Stroe,O., Wood,G., Laydon,A., *et al.* (2022) AlphaFold Protein Structure Database: massively expanding the structural coverage of protein-sequence space with high-accuracy models. *Nucleic Acids Res.*, **50**, D439–D444.

50. Crooks,G.E., Hon,G., Chandonia,J.-M. and Brenner,S.E. (2004) WebLogo: a sequence logo generator. *Genome Res.*, **14**, 1188–1190.

51. Jeffery,C.J. (1999) Moonlighting proteins. *Trends Biochem. Sci.*, **24**, 8–11.

52. Lutkenhaus,J. (1993) FtsZ ring in bacterial cytokinesis. *Mol. Microbiol.*, **9**, 403–409.

53. Coltharp,C. and Xiao,J. (2017) Beyond force generation: Why is a dynamic ring of FtsZ polymers essential for bacterial cytokinesis? *Bioessays*, **39**, 1–11.

54. Ortiz,C., Natale,P., Cueto,L. and Vicente,M. (2016) The keepers of the ring: regulators of FtsZ assembly. *FEMS Microbiol. Rev.*, **40**, 57–67.

55. Mingorance,J., Rivas,G., Vélez,M., Gómez-Puertas,P. and Vicente,M. (2010) Strong FtsZ is with the force: mechanisms to constrict bacteria. *Trends Microbiol.*, **18**, 348–356.

56. Dyer,N. (2009) Tubulin and its prokaryotic homologue FtsZ: a structural and functional comparison. *Sci. Prog.*, **92**, 113–137.

57. Mukherjee,A., Cao,C. and Lutkenhaus,J. (1998) Inhibition of FtsZ polymerization by SulA, an inhibitor of septation in Escherichia coli. *Proc. Natl. Acad. Sci. U. S. A.*, **95**, 2885–2890.

58. Justice,S.S., García-Lara,J. and Rothfield,L.I. (2000) Cell division inhibitors SulA and MinC/MinD block septum formation at different steps in the assembly of the Escherichia coli division machinery. *Mol. Microbiol.*, **37**, 410–423.

59. Burby,P.E. and Simmons,L.A. (2020) Regulation of cell division in bacteria by monitoring genome integrity and DNA replication status. *J. Bacteriol.*, **202**.

60. Wu,L.J. and Errington,J. (2004) Coordination of cell division and chromosome segregation by a nucleoid occlusion protein in Bacillus subtilis. *Cell*, **117**, 915–925.

61. Bernhardt,T.G. and de Boer,P.A.J. (2005) SlmA, a nucleoid-associated, FtsZ binding protein required for blocking septal ring assembly over Chromosomes in E. coli. *Mol. Cell*, **18**, 555–564.

62. Tonthat,N.K., Arold,S.T., Pickering,B.F., Van Dyke,M.W., Liang,S., Lu,Y., Beuria,T.K., Margolin,W. and Schumacher,M.A. (2011) Molecular mechanism by which the nucleoid occlusion factor, SlmA, keeps cytokinesis in check. *EMBO J.*, **30**, 154–164.

63. Wu,L.J., Ishikawa,S., Kawai,Y., Oshima,T., Ogasawara,N. and Errington,J. (2009) Noc protein binds to specific DNA sequences to coordinate cell division with chromosome segregation. *EMBO J.*, **28**, 1940–1952.

64. Egan,A.J.F. and Vollmer,W. (2013) The physiology of bacterial cell division. *Ann. N. Y. Acad. Sci.*, **1277**, 8–28.

65. Wang,M., Fang,C., Ma,B., Luo,X. and Hou,Z. (2020) Regulation of cytokinesis: FtsZ and its accessory proteins. *Curr. Genet.*, **66**, 43–49.

66. Harry,E., Monahan,L. and Thompson,L. (2006) Bacterial cell division: the mechanism and its precison. *Int. Rev. Cytol.*, **253**, 27–94.

67. Miles,Z.D., McCarty,R.M., Molnar,G. and Bandarian,V. (2011) Discovery of epoxyqueuosine (oQ) reductase reveals parallels between halorespiration and tRNA modification. *Proc. Natl. Acad. Sci. U. S. A.*, **108**, 7368–7372.

68. Rio,D.C., Ares,M.,Jr, Hannon,G.J. and Nilsen,T.W. (2010) Purification of RNA using TRIzol (TRI reagent). *Cold Spring Harb. Protoc.*, **2010**, db.prot5439.

69. Keseler,I.M., Gama-Castro,S., Mackie,A., Billington,R., Bonavides-Martínez,C., Caspi,R., Kothari,A., Krummenacker,M., Midford,P.E., Muñiz-Rascado,L., *et al.* (2021) The EcoCyc database in 2021. *Front. Microbiol.*, **12**, 711077.

70. Waterhouse,A.M., Procter,J.B., Martin,D., Clamp,M. and Barton,G.J. (2009) Jalview Version 2 - A multiple sequence alignment editor and analysis workbench. *Bioinformatics*, **25**, 1189–1191.

71. Schneider,T.D. and Stephens,R.M. (1990) Sequence logos: a new way to display consensus sequences. *Nucleic Acids Res.*, **18**, 6097–6100.

72. PyMOL.

73. Bullock,W.O. (1987) XL1-blue : a high efficiency plasmid transforming recA Escherichia coli strain with beta-ga-lactosidase selection. *Biotechniques*, **5**, 376.

74. Galli,E. and Gerdes,K. (2010) Spatial resolution of two bacterial cell division proteins: ZapA recruits ZapB to the inner face of the Z-ring. *Mol. Microbiol.*, **76**, 1514–1526.

75. Amann,E., Ochs,B. and Abel,K.J. (1988) Tightly regulated tac promoter vectors useful for the expression of unfused and fused proteins in Escherichia coli. *Gene*, **69**, 301–315.